Oxide-ion and proton conducting electrolyte materials for clean energy applications: structural and mechanistic features

Lorenzo Malavasi,*[a] Craig A. J. Fisher[b] and M. Saiful Islam*[c]

Received 23rd February 2010
DOI: 10.1039/b915141a

This *critical review* presents an overview of the various classes of oxide materials exhibiting fast oxide-ion or proton conductivity for use as solid electrolytes in clean energy applications such as solid oxide fuel cells. Emphasis is placed on the relationship between structural and mechanistic features of the crystalline materials and their ion conduction properties. After describing well-established classes such as fluorite- and perovskite-based oxides, new materials and structure-types are presented. These include a variety of molybdate, gallate, apatite silicate/germanate and niobate systems, many of which contain flexible structural networks, and exhibit different defect properties and transport mechanisms to the conventional materials. It is concluded that the rich chemistry of these important systems provides diverse possibilities for developing superior ionic conductors for use as solid electrolytes in fuel cells and related applications. In most cases, a greater atomic-level understanding of the structures, defects and conduction mechanisms is achieved through a combination of experimental and computational techniques (217 references).

1 Introduction

A major worldwide challenge is the development of cleaner, sustainable sources of energy to deal with the environmental threat of global warming and the finite nature of fossil fuel reserves. There is, however, no single solution. Promising energy conversion and storage technologies, including fuel cells and lithium batteries, are being developed to help cut carbon dioxide emissions. The performance of these energy systems depends crucially on the properties of their component materials, thus requiring the development of innovative materials chemistry.

One leading technology for future power generation is the solid oxide fuel cell (SOFC). An SOFC is an electrochemical device which converts chemical energy into electricity and, in the simplest case, is based on the chemical reaction between hydrogen (at the anode) and oxygen (at the cathode) to produce water. The two electrode compartments are separated by the electrolyte, which serves as a barrier to gas diffusion but allows ion transport of either oxide ions or protons.

[a] *Department of Physical Chemistry, IENI-CNR and INSTM, University of Pavia, Viale Taramelli, 16, I 27100, Pavia, Italy. E-mail: lorenzo.malavasi@unipv.it*
[b] *Nanostructures Research Laboratory, Japan Fine Ceramics Center, 2-4-1 Mutsuno, Atsuta-ku, Nagoya 456-8587, Japan. E-mail: c_fisher@jfcc.or.jp*
[c] *Department of Chemistry, University of Bath, Bath, UK BA2 7AY. E-mail: m.s.islam@bath.ac.uk*

Lorenzo Malavasi

Lorenzo Malavasi obtained his PhD in chemistry in 2003. He is presently Assistant Professor at the Physical Chemistry Department of the University of Pavia. He was the recipient of the Young Scientist Award for outstanding work in the field of perovskites at the International Conference on Perovskites held in late 2005 in Zürich, of the "Alfredo di Braccio" Prize for Chemistry 2008 of Accademia Nazionale dei Lincei awarded to distinguished under 35-year-old chemists and contributed the Journal Materials Chemistry "Emerging Investigator" issue in 2010. He is working in several areas of solid-state chemistry with particular interest in the investigation of structure–properties correlation in different kinds of functional oxides, in particular electrolyte materials for energetics, magnetic oxides and high-temperature superconductors.

Craig A. J. Fisher

Craig Fisher is a researcher in the Nanostructures Research Laboratory of the Japan Fine Ceramics Center in Nagoya. He obtained his BEng (1992) from the University of New South Wales, Sydney, and DPhil in Materials Science (1996) from the University of Oxford under Professors Adrian Sutton FRS and Sir Richard Brook OBE. He has previously worked at the Australian Nuclear Science and Technology Organisation (ANSTO), as well as in the research group of Saiful Islam at the University of Surrey and University of Bath. His chief interests are in the atomic-scale modelling of materials for electrochemical applications such as fuel cells and lithium ion batteries, with a particular focus on interface phenomena.

Schematics of SOFCs utilizing oxide-ion conducting and proton conducting electrolytes are shown in Fig. 1(a) and (b), respectively.

SOFCs are of particular interest because of their high efficiency (compared to combustion-based technologies), low emissions and fuel flexibility; the latter allows them to use hydrocarbon fuels and hence act as a bridging technology between hydrocarbon- and future hydrogen-based economies.[1,2] They usually operate between 800 and 1000 °C, and the available operating temperature range strongly depends on the characteristics of the anode, cathode and electrolyte materials. Target ionic conductivities for the electrolyte at operating temperatures typically exceed 0.1 S cm^{-1}.

One important challenge in improving SOFC technology is to reduce the working temperature to 500–700 °C. Such intermediate-temperature SOFCs would hasten implementation of this technology in distributed combined heat and power (CHP) systems.[1,2] In addition, lowering the working temperature is advantageous in terms of long-term operation, materials stability, cost and safety.

The role of materials science is fundamental for discovering and developing electrolyte materials that support high ion conductivities (and negligible electronic conductivities) at lower temperatures, together with good chemical stability and sinterability for fabrication. Such breakthroughs underpin applied research, and depend simultaneously upon exploring new classes of compounds and gaining a greater understanding of the structural and mechanistic features of fast-ion conductors at the atomic level.

Intense research in this field, particularly over the last decade, has led to the discovery of several new classes of materials with excellent ion conducting properties, which in some cases exhibit different conduction mechanisms than the vacancy-mediated transport of well-known oxide-ion conductors such as yttria-stabilized zirconia (YSZ). This has triggered a vast amount of research aimed not only at improving performance but also at understanding phenomena on a fundamental level by experimental and theoretical methods.

M. Saiful Islam

Saiful Islam grew up in London and studied Chemistry at University College London, completing his PhD in 1987 with Professor Richard Catlow FRS, followed by a Postdoctoral Fellowship at the Eastman Kodak Labs in Rochester, New York. He then returned to the UK to the University of Surrey, and in 2006 he was appointed Professor of Computational Materials Chemistry at the University of Bath. Saiful's research interests lie in the field of inorganic materials chemistry, focusing on fuel cell and lithium battery materials. He has served on the Editorial Board of the Journal of Materials Chemistry and, in 2008, he was awarded the RSC Francis Bacon Medal—Fuel Cell Science Award.

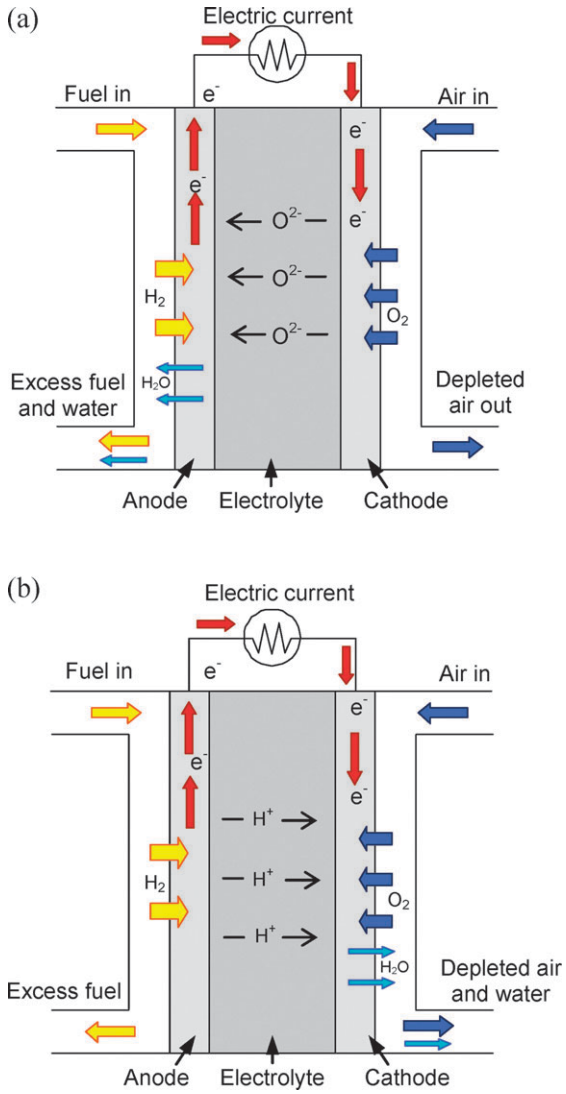

Fig. 1 Schematic diagram of the processes taking place in a solid oxide fuel cell (SOFC) during operation; (a) oxide-ion conducting electrolyte, and (b) proton conducting electrolyte. A key advantage of SOFCs is that they also allow hydrocarbons to be used as a fuel source.

Although numerous examples will be cited, it is beyond the scope of this review to give an exhaustive summary of all the innovative studies in this highly active field. Nor is it intended to be a comprehensive review of fuel cell technology, as excellent reviews on SOFCs,[1,2] polymer electrolyte membrane (PEM) fuel cells[4] and solid acid fuel cells (SAFCs)[5] can be found elsewhere. Rather, this review focuses on electrolyte materials for use in SOFCs, providing first a brief overview of state-of-the-art oxide-ion and proton conducting oxides, and then detailing recent developments regarding new classes of materials, with particular emphasis on their structural and mechanistic features.

2 Conventional oxide-ion conductors

2.1 Fluorite-structured oxides

Most conventional fast oxide-ion conducting materials have crystal structures of the fluorite type, AO_2, where A is a tetravalent cation.[1–3] In this structure, illustrated in Fig. 2,

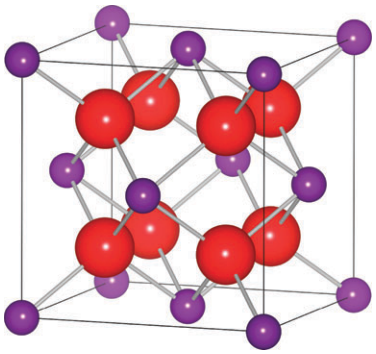

Fig. 2 The fluorite crystal structure (AO_2) adopted by ZrO_2 and CeO_2. The cubic ZrO_2 structure can be stabilized to room temperature by doping. Large red spheres represent O^{2-} ions and small purple spheres A^{4+} ions.

the cations occupy face-centred positions in a cubic unit cell with anions in the eight tetrahedral sites between them.

The best known fluorite-type oxide-ion conductor is acceptor-doped ZrO_2. Pure zirconia is not a good ion conductor, and only adopts the cubic fluorite symmetry above 2300 °C.[6] To stabilize the cubic structure at lower temperatures and to increase the concentration of oxygen vacancies (which are required for ion conduction *via* vacancy hopping), acceptor dopants are introduced onto the cation sublattice.[7–11] This can be described using Kröger–Vink notation,

$$MO + Zr_{Zr}^{\times} + O_O^{\times} \rightarrow M_{Zr}'' + V_O^{\bullet\bullet} + ZrO_2 \qquad (1)$$

$$R_2O_3 + 2Zr_{Zr}^{\times} + O_O^{\times} \rightarrow 2R_{Zr}' + V_O^{\bullet\bullet} + 2ZrO_2 \qquad (2)$$

in which M is a divalent cation, R is a trivalent cation, and $V_O^{\bullet\bullet}$ is a compensating oxygen vacancy. Typical subvalent dopants (*i.e.*, acceptors) are Ca^{2+} and Y^{3+}, producing calcia-stabilized zirconia (CSZ) and yttria-stabilized zirconia (YSZ), respectively, the latter exhibiting good oxide-ion conductivity above about 700 °C.[1–3]

A plot of the conductivity of YSZ is presented in Fig. 3 (together with several other materials which will be discussed later in this article). YSZ is the most common oxide electrolyte material, and has been the mainstay of progress towards commercially viable SOFCs for some time.[1,2] However, its high working temperature (typically 800–1000 °C) makes it problematic for use in small-scale applications.[12] Extensive research has also been carried out into Sc-doped ZrO_2 (ScSZ), which exhibits superior ionic conductivity,[13] but its use is limited on account of the high cost of scandium.

Another fluorite-type conductor is doped CeO_2.[14–19] Typical dopants include Gd_2O_3 (producing gadolinia-doped ceria, GDC, also known as cerium–gadolinium oxide, CGO) and Sm_2O_3 (producing samaria-doped ceria, SDC, also known as cerium–samarium oxide, CSO). These solid solutions have conductivities which are significantly higher than that of YSZ, particularly at lower temperatures (500–700 °C). These tantalizingly high conductivities suggest they can be used to reduce the operating temperature of SOFCs. However, at low oxygen partial pressures and temperatures above *ca.* 600 °C the conductivity of these materials is not purely ionic, with a non-negligible proportion of electronic (n-type) conductivity,

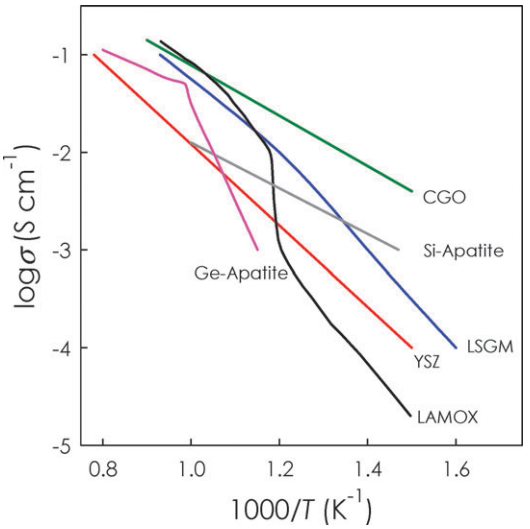

Fig. 3 Total conductivities of several well-known oxide-ion conductors as a function of inverse temperature: YSZ, $(ZrO_2)_{0.92}(Y_2O_3)_{0.08}$;[3] CGO, $Ce_{0.8}Gd_{0.2}O_{1.9}$;[27] LSGM, $La_{0.9}Sr_{0.1}Ga_{0.8}Mg_{0.2}O_{2.85}$;[47] LAMOX, $La_2Mo_2O_9$,[64] Si-apatite, $La_{10}(SiO_4)_6O_3$,[84] and Ge-apatite, $La_{10}(GeO_4)_6O_3$.[84]

consistent with the partial reduction of Ce^{4+} to Ce^{3+}.[20] For example, 10 mol% Gd-doped ceria has been found to possess greater stability in reducing atmospheres than 20 mol% Gd-doped ceria. Attempts to improve the material's redox stability through co-doping with other rare earths have so far had limited success;[21] ionic conductivities greater than that of 10 mol% GDC have been reported for co-doping with Sm and Nd,[22] although the improvement does not appear great.

Despite these difficulties, it has been demonstrated that an SOFC can be successfully operated with a ceria solid electrolyte at a working temperature of 500–700 °C, as the electronic contribution does not affect greatly the overall cell performance, except for an obvious reduction in the total voltage generated.[23] Even at these lower temperatures, the ionic transference number of CGO ($t_O > 0.9$) is sufficiently high to provide good fuel cell efficiency.[23] Typical oxide-ion conductivity values as a function of reciprocal temperature for $Ce_{0.8}Gd_{0.2}O_{1.9}$[24] are given in Fig. 3.

Increasing the concentration of Gd_2O_3, Yb_2O_3 or La_2O_3 beyond about 11–14 mol% in CeO_2 leads to lower ion conductivities.[25] A combination of atomistic simulation[26] and experimental studies[28,29] has shown that strong defect association or clustering occurs between the dopant ions and oxygen vacancies. Early modelling work[26] indicated that a key factor for the interaction between these defects is the elastic strain introduced into the lattice by size mismatch between the dopant and host cation. Recently, however, systematic comparison of conductivities of 10 mol% trivalent cation-doped cerias has suggested that structure–property relationships are more complex, and that the observed trends in ionic conductivity cannot be explained in terms of minimum elastic strain alone.[30]

An alternative strategy for improving the properties of fluorite-type oxide ion conductors is to add zirconia to ceria (or *vice versa*). As these two fluorite oxides are mutually soluble, the wide range of dopants available means there is

enormous scope for developing better electrolytes by taking advantage of zirconia's superior chemical and mechanical properties while retaining the high ion conductivity of ceria.[31]

Another important fast oxide-ion conductor with a fluorite based structure is δ-Bi_2O_3.[1–3,32,33] This compound is characterized by an oxygen sublattice with a high fraction of vacancies, which is the basis for its high ion conductivity. However, the highly conductive δ phase is only stable above *ca.* 730 °C. Stabilization of this phase to room temperature can be achieved by partially replacing bismuth with rare-earth elements (such as Y, Dy or Er) in combination with supervalent cations, such as Nb or W.[34–39] Similar to ZrO_2-based electrolytes, the highest ionic conductivities are achieved for materials containing the minimum dopant concentration required to stabilize the cubic fluorite structure. However, in many cases the doping level required is high (15–42 mol%), resulting in relatively poor conductivities, especially at low temperatures. An exception to this phenomenon has been found for some Re- and rare-earth-doped Bi_2O_3 compositions, which display exceptionally high oxide-ion conductivities even at low temperature.[40]

Renewed interest in δ-Bi_2O_3 has mainly focussed on the local structure and ion migration paths using new characterisation techniques such as neutron total scattering.[41] This has revealed that, even though the long-range order evident from conventional X-ray or neutron diffraction is consistent with a cubic symmetry, the local structure of the δ phase closely resembles the distorted square pyramidal arrangement found within the phase of the pure material stable at ambient temperature, otherwise known as the α phase.[41] It has been argued that the asymmetric electron density around the Bi^{3+} ion is crucial for promoting extensive anion disorder within δ-Bi_2O_3, with the ion diffusion facilitated both by the flexible cation sublattice and substantial relaxation of the surrounding anions.[41]

Some doubt remains regarding the ability of δ-Bi_2O_3 to maintain high ionic conductivity at typical working temperatures (~500 °C) for long periods of time. Recent work has tried to clarify this situation, seeking optimal dopant concentrations that provide both high conductivity and long term stability.[42]

Other fluorite-related materials include the pyrochlore structure with general composition $A_2B_2O_7$.[43] This can be viewed as a superstructure of a defective fluorite, $(A,B)O_{1.75}$, with one oxide-ion vacancy per formula unit, yielding a vacancy concentration of 12.5 mol%. The systems most widely studied are $Gd_2(Ti_{1-x}Zr_x)_2O_7$[44] and $Gd_{2-y}Ln_yZr_2O_7$ (where Ln = Sm, Nd, La).[45] However, the oxide-ion conductivities of pyrochlore materials are still below those obtained for YSZ and CGO, and their use in SOFCs is currently not practical.

2.2 Perovskite-structured oxides

In the ABO_3 perovskite structure, illustrated in Fig. 4, the large A cation is coordinated to twelve anions, with the B cation occupying a six-coordinate site, forming a network of corner-sharing BO_6 octahedra. Tilting of these octahedra leads to deviations from the ideal cubic symmetry.

A widely studied perovskite-structured oxide with possible applications in intermediate-temperature SOFCs is doped lanthanum gallate, $LaGaO_3$. The high ion conductivity of (Sr,Mg)-doped $LaGaO_3$, of general formula

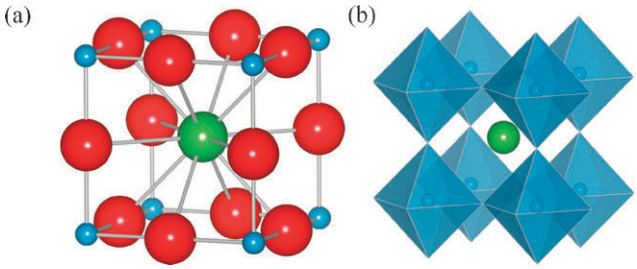

Fig. 4 Two representations of the cubic perovskite structure of $LaGaO_3$; (a) La-centred unit cell, and (b) corner-shared GaO_6 octahedra with La centred on 12-coordinate sites. Large red spheres are O^{2-} ions, light green spheres La^{3+} ions and small blue spheres Ga^{3+}.

$La_{1-x}Sr_xGa_{1-y}Mg_yO_{3-\delta}$ (often termed LSGM), was first reported in 1994 by Ishihara *et al.*,[46] and by Feng and Goodenough.[47] This material exhibits pure ionic conductivity over a very wide range of oxygen partial pressure ($10^{-20} < pO_2 < 1$), with values higher than those of YSZ even at relatively low temperatures for composition $La_{0.9}Sr_{0.1}Ga_{0.8}Mg_{0.2}O_{3-\delta}$,[1–3,48,49] as shown in Fig. 3.

Use of LSGM as an electrolyte has so far been hampered by several issues, such as difficulty in obtaining single phase materials,[50] the volatility of gallium at high temperatures, and its high reactivity with Ni (typically used as the anode), the latter resulting in formation of the ionically-insulating $LaNiO_3$ phase.[48,51] Again, the purpose of acceptor doping on both the La site (with Sr) and Ga site (with Mg) is the creation of oxygen vacancies to promote rapid oxide-ion conductivity, *e.g.*,

$$2SrO + 2La_{La}^{\times} + O_O^{\times} \rightarrow 2Sr_{La}^{'} + V_O^{\bullet\bullet} + La_2O_3 \qquad (3)$$

It should be stressed that even though X-ray diffraction (XRD) of LSGM indicates a cubic crystal structure,[46] neutron diffraction reveals a monoclinic structure.[52] From extensive *in situ* neutron diffraction studies it has been determined that simultaneous Sr and Mg doping leads to a reduction of the tilt of the GaO_6 octahedra with respect to the parent compound (and with respect to the Mg-only-doped phase). This increased symmetry promotes greater oxide-ion conductivity.[53]

The defect chemistry and migration path of oxide ions in lanthanum gallates has been examined using computational techniques,[54,55] which reveal that migration occurs by vacancy hopping between oxygen sites along a GaO_6 octahedron edge, with a slightly curved trajectory accompanied by outward relaxation of adjacent cations. This mechanism is illustrated in Fig. 5(a). The calculated migration path was later confirmed experimentally by Yashima *et al.*[56] using the maximum-entropy method (MEM) based on neutron diffraction data for the optimal composition $(La_{0.8}Sr_{0.2})(Ga_{0.8}Mg_{0.15}Co_{0.05})O_{2.8}$, as shown in Fig. 5(b).

In comparison to the fluorite oxides, there have been fewer studies on defect clustering in perovskite oxides. Atomistic modelling of doped $LaGaO_3$,[54,57] however, suggests that the negligible binding energy for Sr dopant-vacancy clusters may be a major factor in promoting the observed high oxide-ion conductivity. In contrast, Mg-vacancy clusters have significant binding energies, suggesting greater vacancy trapping. This is

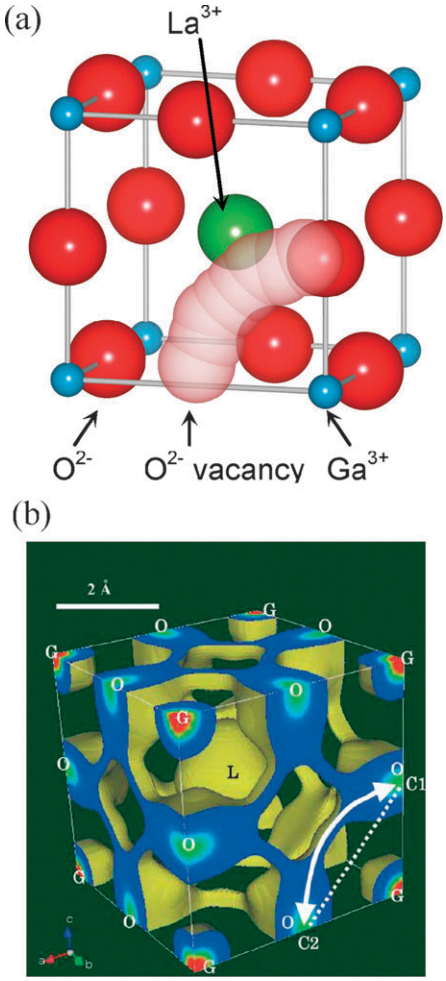

Fig. 5 (a) Schematic representation of the curved path for oxygen vacancy migration in the [Ga–O] plane of $LaGaO_3$;[54] (b) equicontour surface of scattering amplitude in cubic $(La_{0.8}Sr_{0.2})(Ga_{0.8}Mg_{0.15}Co_{0.05})O_{2.8}$ at 1665 K. L, G and O denote the A-site cations (La or Sr), B-site cations (Ga, Mg or Co) and oxide ions, respectively. Reprinted with permission from ref. 56, copyright Elsevier, 2003.

consistent with the observed increase in activation energy for ion migration at higher Mg doping levels in $La_{1-x}Sr_xGa_{1-y}Mg_yO_{3-\delta}$,[58] and would lead to two distinct regions or non-linear portions in the conductivity Arrhenius plot. Such a change in slope is indeed observed experimentally.[59]

Despite reducing the ionic transport number, t_O (also known as the transference number), slightly, replacement of Mg with less binding dopants, such as Co or Ni, has been found to be beneficial to the overall performance of these materials.[60] Studies of honeycomb-type SOFCs using such electrolytes have demonstrated high power densities.[61]

Other perovskites known to exhibit oxide-ion conductivities comparable to that of YSZ include $NdGa_{0.9}Mg_{0.1}O_{2.95}$[62] and $Gd_{0.85}Ca_{0.15}AlO_{2.925}$.[63] The wide range of solid solubilities and variety of compositions means these and other perovskite systems warrant continued investigation.

Work is also being carried out on perovskite-related oxides of the K_2NiF_4 ($A_2BO_{4+\delta}$) structure such as $Ln_2NiO_{4+\delta}$ (where Ln = La, Nd, Pr). In these materials, excess oxygen ($\delta > 0$) is accommodated at interstitial sites with oxide-ion conduction mediated by an interstitial transport mechanism.[64] Although not pure oxide-ion conductors (to date all are mixed ionic/electronic conductors being considered for use as SOFC cathodes), altering the chemistry to suppress the electronic conductivity would open up another field of oxide-ion conducting electrolyte research.

3. New oxide-ion conductors

As described above, several conventional materials with good ionic conductivity are known and some are already in practical use. However, several drawbacks, such as high operating temperatures, partial electronic conductivity and/or poor chemical stability, still limit their widespread application. These issues have motivated researchers in the solid-state ionics community to develop new materials with improved properties. In this section we highlight the most recent advances in the development of novel oxide-ion conducting materials.

3.1 $La_2Mo_2O_9$ (LAMOX)

In 2000, Lacorre and co-workers reported a new family of fast oxide-ion conductors based on the parent compound $La_2Mo_2O_9$ (LAMOX).[65] This compound exhibits a first-order phase transition from the non-conductive monoclinic phase (α) to the highly-conductive cubic phase (β) at around 580 °C, with the latter having an ionic conductivity of 6×10^{-2} S cm^{-1} at 800 °C. Conductivity data for pure LAMOX[66] is included in Fig. 3.

The structure of the low-temperature (α) polymorph was solved by Evans *et al.*[67] This compound has one of the most complex crystal structures so far reported, with 312 crystallographically distinct sites. The structure of the high-temperature cubic form was first proposed in 2000 by Lacorre *et al.*[65] and then revised in 2001.[68] Based on results from neutron diffraction, a model was proposed in which two of the three available oxygen sites (labelled O2 and O3) are partially occupied and characterized by huge thermal displacement parameters, B (*e.g.*, B_{eq} up to ~20 Å^2 for the O3 site). The presence of a strong modulation in the neutron diffraction patterns of the conducting β phase led to the conclusion that there is substantial disorder on the oxygen sublattice;[65,68] this disorder is considered to be the origin of the high oxygen mobility.

The structure of β-LAMOX shown in Fig. 6 (after O'Keeffe and Hyde)[69] emphasises the coordination environments of the anions. A rigid structural framework built up from [La–Mo–O1] tetrahedral units is surrounded by partly delocalized oxide ions on O2 and O3 sites. The [La–Mo–O1] framework contains tunnels parallel to the unit cell axes, in which the O2 and O3 sites lie.

It has been proposed that the structure of the β phase corresponds to a time-averaged version of the room-temperature monoclinic structure of the α phase,[67] as illustrated in Fig. 7. The huge thermal ellipsoids around the Mo ions in the β phase correspond to the independent O sites in α-$La_2Mo_2O_9$. This view was confirmed by neutron pair distribution function (PDF) analysis, which showed that the transition from monoclinic to cubic symmetry involves a change from a static

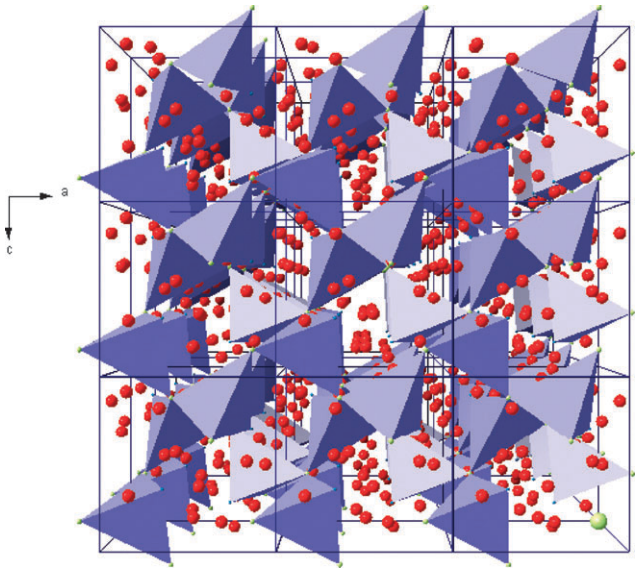

Fig. 6 β-$La_2Mo_2O_9$ viewed as a rigid framework of [La–Mo–O1] units with O2 and O3 sites located within the channels. Reprinted with permission from ref. 70, copyright Elsevier, 2008.

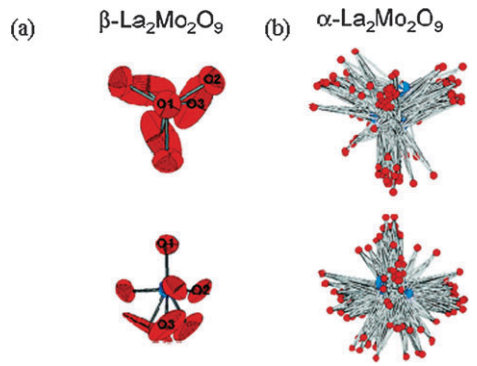

Fig. 7 Correlation between (a) the dynamically disordered oxygen sites in β-$La_2Mo_2O_9$, and (b) the static O distribution in α-$La_2Mo_2O_9$. For α-$La_2Mo_2O_9$, the picture represents a superposition of all independent Mo atoms and their coordination spheres obtained by transformation of the monoclinic superstructure into the underlying cubic subcell. Reproduced with permission from ref. 67, copyright American Chemical Society, 2005.

to a dynamic distribution of the oxygen defects while the local monoclinic structure is preserved.[71]

Overall, the partial occupancies of the O2 and O3 sites and the very short distances between these pairs of atoms are believed to facilitate the easy oxygen migration throughout this structure. Mechanical and dielectric relaxation studies suggest a possible path for long-range diffusion of oxide ions in β-LAMOX; this involves the oxide ions or vacancies jumping from the O1 site (fully occupied) to an O2 site, then to an O3 site, and again to an O1 site, a pathway which is three-dimensional in nature.[72] However, a complete picture of the conduction mechanism in this complex oxide is still lacking.

Although pure LAMOX has a high oxide-ion conductivity (in the cubic phase), in order for it to be considered as a practical material for solid electrolyte applications, two issues need to be addressed: the structural phase transition (at about 580 °C), resulting in significant volume strains, and the low chemical stability under reducing conditions.

Doping pure LAMOX with alkaline (*e.g.*, K and Rb) and alkaline-earth (*e.g.*, Ca, Sr and Ba) cations on the La site stabilizes the cubic phase at room temperature without significantly affecting the conductivity.[70,73–75] Measurements of oxygen tracer diffusion coefficients in Gd-, Y- and Nd-substituted (La site) and W-substituted (Mo site) samples[76] have demonstrated that the diffusion coefficients of these compositions are higher than those of YSZ and LSGM.[77]

On the other hand, it has been shown that $La_2Mo_2O_9$ readily reduces in dilute hydrogen, leading to the formation of a mixed valent Mo^{5+}/Mo^{6+} phase, $La_7Mo_7O_{30}$, before eventual decomposition.[78] One way to improve the phase stability under low oxygen pressure, pO_2, appears to be to substitute molybdenum with a less reducible cation. This has been successfully demonstrated for tungsten,[79–83] which has a wide solid solution range in $La_2Mo_2O_9$. In particular, co-doped LAMOXs such as $La_{1.7}Gd_{0.3}Mo_{0.8}W_{1.2}O_9$ have been shown to be stable at low pO_2 with no loss of oxide-ion conductivity. Other studies have shown that several single-doped (particularly alkaline-earth doped) and co-doped phases (with W on the Mo site) undergo demixing–recombination at high temperature (> 700 °C), and suggests that the pure phases are only metastable at room temperature.[76] This effect, which is strongly dependent upon the synthesis route and thermal treatment, may be the source of the wide variation in the solid solution limits reported in the literature.

A systematic study of the phase stability of various doped LAMOX compositions is still needed. Further investigations are required if the potential of this system for use as an electrolyte is to be realized.

3.2 Si and Ge apatites

Apatite-type oxides are among the most fascinating of the new materials being studied as alternative SOFC electrolytes. In the mid-1990s, fast oxide-ion conductivity was discovered in silicate-based apatites $Ln_{9.33}(SiO_4)_6O_2$ (where Ln is typically a large lanthanide ion such as La^{3+} or Nd^{3+}).[84,85] Since then, an increasing number of experimental and computational studies have sought to clarify the structure–property relationships in both Si- and Ge-based systems (for a detailed review see ref. 86).

The general formula for apatite oxides can be written $M_{10}(XO_4)_6O_{2\pm y}$, where M is a rare-earth or alkaline-earth cation, X is a p-block element such as P, Si or Ge, and y is the amount of oxygen non-stoichiometry. These materials are isostructural with the well-known hydroxyapatite biomaterials found in bones and teeth.

The best apatite oxide-ion conductors that have been found to date are the Si- and Ge-based lanthanum apatites. Their crystals typically exhibit hexagonal symmetry (space group $P6_3/m$), with an a lattice parameter 9.7–9.9 Å and c parameter around 7 Å (varying with the type and amount of dopant).[85]

Si(Ge)-based apatites are comprised of isolated $Si(Ge)O_4$ tetrahedra aligned to form two distinct channels running

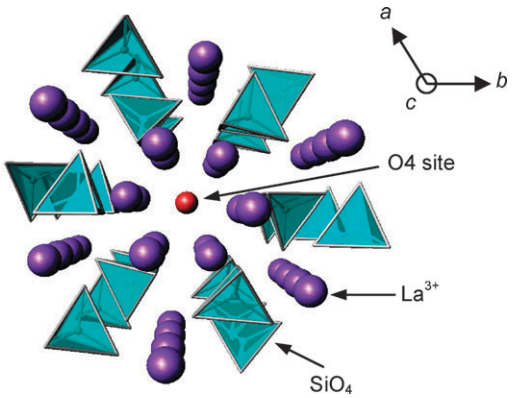

Fig. 8 Apatite structure of $La_{9.33}(SiO_4)_6O_2$ viewed down the *c* axis showing SiO_4 tetrahedra, rows of La2 ions and the La1/O4-containing channels. For clarity, La2 vacancies are not shown.

parallel to the *c* axis (as shown in Fig. 8), with one channel type containing rows of lanthanum (La1) ions in a ring formation with a row of oxide ions at the centre, and the other channel type containing rows of lanthanum (La2) ions alone.

It has been established that the key defects for high ionic conductivity in apatite silicates and germanates are interstitial oxide ions, leading to interstitial-type transport mechanisms. This contrasts with the conventional fluorite (*e.g.*, YSZ, CGO) and perovskite (*e.g.*, LSGM) oxide-ion conductors where oxide-ion transport is by the vacancy-hopping mechanism discussed above.

The carrier species in apatites are purely anionic for most compositions, with high oxygen transference numbers ($t_O > 0.9$) across a wide range of oxygen partial pressures.[87,88] The conductivities are comparable to other electrolytes being considered for SOFC applications (Fig. 3). Particularly high conductivities have been measured parallel to the *c* axis in single crystals, consistent with the anisotropy of the hexagonal structure.[89]

Several strategies are being explored to improve the transport and chemical properties of rare-earth apatite silicates and germanates. For example, it has been shown that the conductivity of $La_{9.33+x}(SiO_4)_6O_{2+3x/2}$ increases as extra oxygen is introduced into the structure ($x > 0$); specifically, the conductivity at 500 °C increases from 1.1×10^{-4} S cm^{-1} for $x = 0$ to 1.3×10^{-3} S cm^{-1} for $x = 0.34$.[90] However, compositions with higher oxygen contents ($x > 0.34$) are not phase pure.

For both Si- and Ge-based systems the range of oxygen non-stoichiometry for which phase-pure materials can be synthesised is relatively narrow; the maximum amount of interstitial oxygen that can be accommodated in the silicate structure without secondary phase formation is lower than that of the germanates (maximum oxygen content of 26.5 per formula unit for silicates *vs.* 27 for germanates).[86]

Stoichiometric compositions in terms of both cations and anions (for example, $La_8M_2(SiO_4)_6O_2$, where M is a divalent cation such as Ca, Sr or Ba) have very low conductivities. An increase of ionic conductivity is usually observed when oxygen excess compounds of general composition $La_9M(SiO_4)_6O_{2.5}$ are produced by increasing the La content while keeping the system cation stoichiometric.[90–92]

The apatite structure allows great flexibility for accommodating a wide range of cation dopants on both the La and Si/Ge sites. This flexibility allows relatively large local distortions and changes in site volumes to be tolerated,[93] making the apatites a very interesting structural type from a chemical substitution point of view. In this review we will outline the most effective doping routes; more detailed overviews of doping strategies for optimising apatite-type ionic conductors can be found in refs. 84, 86, 90 and 93.

The range of dopants that can be introduced on the La site is significantly wider than for most other fast-ion conductors, such as perovskite-type oxides. Doping on the Si site is another useful way of improving conductivity. Lower valent ions tend to increase conductivity, particularly smaller cations such as Mg^{2+}.[86] Isovalent doping on the Si site tends to suppress the conductivity substantially, particularly for Ti-doped silicates;[86,94] trapping of interstitial oxygens by Ti, which prefers a higher coordination sphere, has been proposed to explain this phenomenon, with evidence in support of this view coming from both ^{26}Si nuclear magnetic resonance (NMR) data and computer modelling.[94]

Cation doping (*e.g.* Mg, Ba, Co, Ga) of the germanates has also been extensively examined.[86,87] In contrast to the hexagonal stoichiometric compositions, oxygen excess $La_{9.33+x}(GeO_4)_6O_{2+3x/2}$ has triclinic symmetry; the lower symmetry leads to more strongly bound oxygen, and results in reduced conductivities.[95] The influence of the degree of oxygen excess on the hexagonal–triclinic transition has been confirmed experimentally, since nitridation of oxygen excess triclinic $La_{10}Ge_6O_{27}$ results in the formation of hexagonal anion stoichiometric $La_{10}Ge_6O_{24}N_2$.[96] In order to stabilise the hexagonal lattice while retaining high oxygen contents, doping with Y, *e.g.*, $La_8Y_2Ge_6O_{27}$, has proven effective, leading to enhanced low temperature conductivities compared to other compositions.[97]

As noted, the Si/Ge apatites are interstitial oxide-ion conductors. The precise location of the oxygen interstitial sites and their conduction pathway have stimulated much debate, particularly for the silicate systems. Computer modelling studies[98] identified a favourable interstitial oxide-ion site at the channel periphery neighbouring the SiO_4 units with significant local structural distortions. Subsequent experimental support has been provided by neutron diffraction, solid-state ^{29}Si NMR, synchrotron XRD-MEM and Raman spectroscopy experiments.[86,99–101] Interestingly, the NMR studies[99] have shown a correlation between the ^{29}Si spectra and the conductivity, with poorly conducting samples showing a single NMR resonance (consistent with a single Si environment), whereas in fast-ion conducting compositions, an extra peak is apparent, attributed to a silicate group adjacent to an interstitial oxygen site. There have also been reports of other interstitial sites closer to the oxide channel centre,[102] which may indicate sensitivity of the interstitial site to sample composition and synthesis conditions; these issues need to be clarified by further investigation.

The location of the interstitial oxide ion in the germanates appears to have greater consensus. Both neutron diffraction

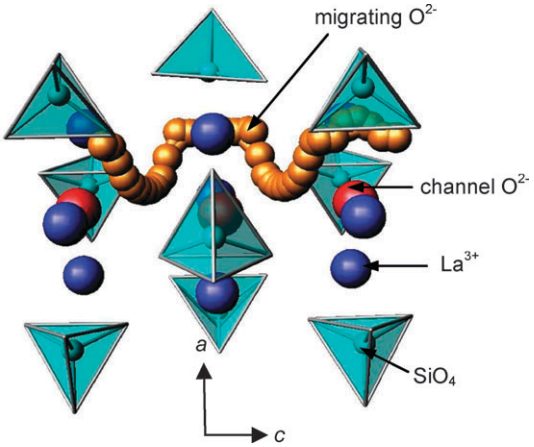

Fig. 9 Interstitial oxide-ion migration along the *c* axis in the $La_{9.33}Si_6O_{26}$ apatite following a nonlinear pathway.[86,98]

and modelling studies indicate it is more closely associated with the GeO_4 units, leading to the formation of five-coordinate Ge sites.[103,104]

One of the most intriguing features of apatite oxide-ion conductors is related to the conduction mechanism. Computer modelling of the non-stoichiometric composition $La_{9.33}Si_6O_{26}$ has shown that oxygen interstitials, present as Frenkel defects, follow a complex sinusoidal trajectory along the periphery of the La2 channels aided by considerable relaxation of the SiO_4 substructure.[98] This mechanism is illustrated in Fig. 9.

Synchrotron XRD studies of $La_{9.71}(Si_{5.81}Mg_{0.18})O_{26.37}$, coupled to whole-pattern fitting based on the maximum-entropy method (MEM), have confirmed the position of the interstitial oxygen near the edge of the La channels, and the covalent nature of the Si–O bonds. Electron density maps are also consistent with migration of oxide ions predominantly in the *c* direction.[101]

Molecular dynamics (MD) simulation of apatite germanates has shown that there are significant differences compared to the silicate systems.[103] This work revealed that O4 ions within the La channels serve as a "reservoir" for the creation of interstitial oxide-ion defects, with ion migration following either a "fan-like" mechanism in the *c* direction, or between adjacent channels (in the *ab* plane) by the formation of Ge_2O_9 units. These results suggest that the conduction mechanism in apatite germanates is more isotropic compared to the strongly one-dimensional migration found in the silicates. Further evidence for such behaviour is provided by experimental data showing that Mg and Bi doping on the La site has less influence on the conductivity in germanates than in the silicates.[86]

The enhanced ionic conductivity of $La_{10-x}(GeO_4)_6O_{3-1.5x}$ materials in wet atmospheres observed by León-Reina *et al.*[105] has been attributed to proton conduction below 873 °C. Further conductivity and modelling studies of Si/Ge apatites (including $La_{9.33}(SiO_4)_6O_2$ and $La_8Ba_2(GeO_4)_6O_2$) suggest that water incorporation is more favourable (exothermic) in the Ge-apatites and leads to additional interstitial oxide ions as well as protonic defects.[106] However, no clear isotope effect has been observed on replacing H_2O with D_2O. Further investigations are thus required to clarify this issue.

In summary, apatite-type silicates and germanates are among the most promising new fast oxide-ion conductors currently known. There are still many avenues to explore in order to further improve their properties, particularly by chemical substitution routes. The development of low-temperature and sol–gel synthesis techniques,[107–109] and optimisation of compatible electrodes will hasten their implementation in SOFC devices, where silicates are preferred because of their lower cost. To date, there are only a few reports of apatite thin film preparation and characterisation,[110–112] although testing of cells containing apatite electrolytes is already underway.[113]

3.3 Tetrahedrally-coordinated gallium oxides

Recently, high oxide-ion conductivity has been reported in various oxides containing GaO_4 tetrahedral units.[114–117] One of these phases, $La_{1-x}Ba_{1+x}GaO_{4-x/2}$, displays both proton conductivity (particularly below 700 °C) and oxide-ion conductivity.[114,115]

The stoichiometric compound $LaBaGaO_4$ possesses the β-K_2SO_4 structure,[114] with Ga in a distorted tetrahedral environment, as illustrated in Fig. 10. Variation of the La/Ba ratio (*i.e.*, varying *x* in $La_{1-x}Ba_{1+x}GaO_{4-x/2}$) results in formation of oxygen vacancies in the lattice. The oxygen vacancies are accommodated by considerable rearrangement of two neighbouring GaO_4 units, to form a Ga_2O_7 group, so that each Ga retains its tetrahedral coordination. The formation of these Ga_2O_7 groups has also been experimentally confirmed by means of neutron diffraction of $La_{0.8}Ba_{1.2}GaO_{3.9}$.[114]

Modelling of oxide-ion migration in this compound has revealed that the lowest energy pathway occurs *via* the breaking and re-forming of the Ga_2O_7 units. The transfer of oxide ions between neighbouring tetrahedra facilitates long-range diffusion.[114] In this respect, the predicted oxide-ion conduction mechanism in $La_{1-x}Ba_{1+x}GaO_{4-x/2}$ is quite unusual and reminiscent of a concerted "cog-wheel"-type motion. A key feature for the transport mechanism is the intrinsic flexibility of the structure, allowing considerable local lattice relaxation.

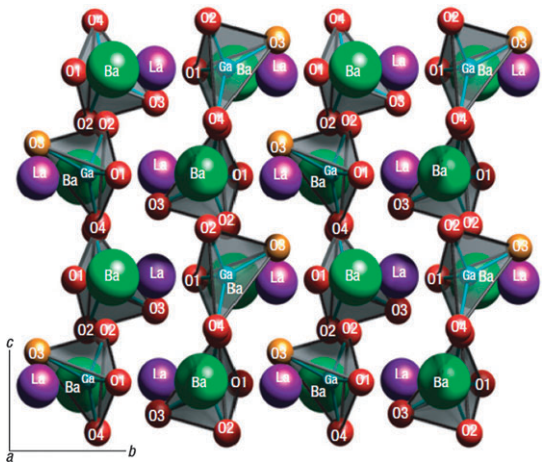

Fig. 10 Crystal structure of $LaBaGaO_4$ comprised of GaO_4 distorted tetrahedra, and ordered alternating layers of lanthanum and barium. The GaO_4 tetrahedra are isolated from one another (with an elongated Ga–O3 bond).

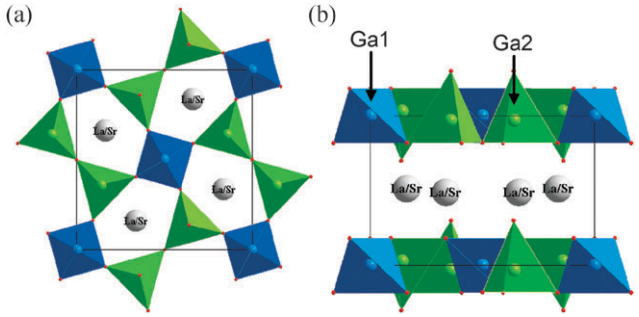

Fig. 11 Melilite structure of $LaSrGa_3O_7$: (a) view along the *c* axis, showing Ga tetrahedra connected through bridging oxygens to form distorted pentagonal rings; (b) view along the *b* axis, showing layered structure with non-bridging oxygens pointing towards the La/Sr layer.[117] Ga atoms occupy two distinct sites: Ga1 (blue) and Ga2 (green).

It is to be expected that similarly high conductivities may be present in other ion conductors containing tetrahedral moieties and flexible structural networks.

More recently, melilite-structured gallates have been proposed as alternative solid electrolyte materials following the discovery of interstitial oxide-ion conductivity in the $LaSrGa_3O_7$-based system.[117] The melilite crystal structure has tetragonal symmetry and is composed of layers of corner-sharing GaO_4 units which are linked to form distorted pentagonal rings (Fig. 11). Along the *c* axis, La and Sr are positioned between GaO_4 layers, aligned with the centres of the pentagonal rings. [118]

The electrical conductivity of the parent compound, $LaSrGa_3O_7$, is relatively low. A large increase is observed, however, by increasing the La/Sr ratio according to $La_{1+x}Sr_{1-x}Ga_3O_{7+x/2}$, thereby introducing an oxygen excess to maintain charge balance.[117,119] The highest electrical conductivity, with an ionic transport number close to 0.95, has so far been achieved for $x = 0.55$–0.56.[117,120] In general, the synthesis of these compositions is not trivial and some care must be taken to produce single-phase samples with $x > 0$. The high conductivities measured testify to the potential of this system for developing suitable solid electrolytes for use in SOFCs.

The positions of the extra oxygen introduced into the structure by altering the La/Sr ratio have been identified using neutron diffraction and are found to lie within the tetrahedral layers in the same plane as the Ga ions. The presence of the large La/Sr cations between GaO_4 layers in the voids bounded by pentagonal rings limits the possibility of oxide-ion migration along the *c* axis.

Structural investigations[117] have shown that these interstitial oxygens are responsible for the higher oxide-ion conductivity of $La_{1.54}Sr_{0.46}Ga_3O_{7.27}$ compared to $LaSrGa_3O_7$, although the precise transport mechanism in this system has yet to be established. Results of an MD study[121] suggest that migration occurs by an "interstitialcy" or cooperative-type mechanism involving the concerted knock-on motion of interstitial and lattice oxide ions within the Ga layers.

A common feature of these gallium-based ion conductors is the flexibility of the structural networks, in which the coordination number of the Ga ions can change readily. Hence flexibility and ease of deformation of the Ga–O polyhedra appear to be important factors favourable to rapid oxide-ion migration in these systems.

3.4 Other related materials

Mayenite. Mayenite, nominal composition $Ca_{12}Al_{14}O_{33}$, was first reported to be a fast oxide-ion conductor twenty years ago,[122] and is once again attracting attention as a cost-effective electrolyte for a number of applications. The crystal structure of this material (space group $I\bar{4}3d$, $Z = 2$, $a = 11.98$ Å) consists of 64 oxygens contained within the Ca–Al–O framework and two extra-lattice oxide ions randomly occupying one-sixth of the cages thus formed.[123,124] A representation of this cage structure highlighting the position of the extra-lattice oxygen is shown in Fig. 12.

Recent detailed studies using high-temperature neutron diffraction have suggested a model for oxygen diffusion based on a jump-like process involving exchange of the extra-lattice oxygen with framework oxygens, intimately coupled to large relaxations of the nearest neighbour Ca ions and, possibly, the other ions in the cage walls.[123] Under reducing conditions a small concentration of electronic species turns mayenite into an electronic conductor. However, owing to their complex defect chemistry, the nanocages have the unusual property of becoming less electronically conducting as the water content increases.[124]

The renewed interest in this structure as a solid electrolyte arises from its ability to accommodate a range of other anions, thus offering the possibility of preparing nitride- or fluoride-ion conductors. As of yet, a complete picture of the atomic-scale migration mechanisms has not been achieved. This poorly understood system therefore merits further detailed investigation.

BIMEVOX. As mentioned in section 2.1, δ-Bi_2O_3 displays extremely good oxide-ion conductivity but suffers from phase stability problems, particularly in reducing atmospheres. A more stable and better ion-conducting family of oxides is based on a related system, with parent oxide $Bi_4V_2O_{11}$.[125,126] This is a layered material showing complex polymorphism, the main two polymorphic transitions of which are $\alpha \rightarrow \beta$ (at 447 °C) and $\beta \rightarrow \gamma$ (at 567 °C).[126] Substitution of V by a host of iso- and aliovalent cations leads to stabilization of the highly conducting γ polymorph at room temperature, with

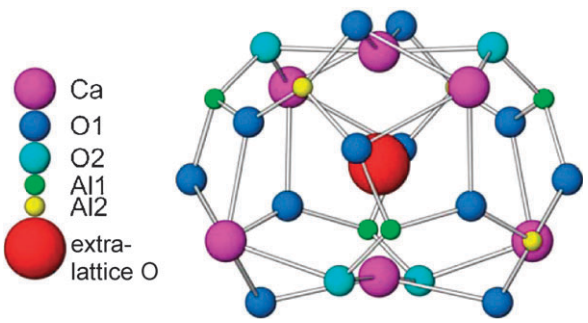

Fig. 12 A mayenite cage containing an extra-lattice oxygen. Reprinted with permission from ref. 123.

conductivities on the order of 0.1–1.0 S cm^{-1} at 600 °C. This family of solid electrolytes is known as the BIMEVOXs where BI stands for bismuth, ME for metal, V for vanadium and OX for oxygen.[127]

The crystal lattice of this structural family is based on the Aurivillius series and consists of alternating $Bi_2O_2^{2+}$ and perovskite-like $VO_{3.5}^{2-}$ layers, with oxygen vacancies in the perovskite layers facilitating rapid ion migration. High resolution ^{17}O and ^{51}V magic angle spinning (MAS) NMR spectroscopy studies[128] of $Bi_4V_2O_{11}$ have shown that oxide-ion conduction involves anions in the V–O layers with the most mobile ions associated with the more distorted $VO_{3.5}$ groups. Similar ^{17}O two-dimensional NMR studies of the related Nb-doped Bi_2WO_6 material have revealed the oxide-ion conduction pathways.[129]

The most common dopants added to BIMEVOXs are Cu, Ni, Co, and Mg, which not only stabilise the highly conductive γ structure at lower temperatures, but also result in an ionic transport number close to 1.0 for temperatures up to about 630 °C.[130–139] Interest in the BIMEVOX compounds is still active because of their good conductivity, although problems with their high chemical reactivity, reducibility and low mechanical strength have yet to be adequately addressed.

Apart from its potential as a solid electrolyte for SOFCs, BIMEVOX has been successfully used as an electrochemical catalyst for selective reduction of NO because of its high conductivity at relatively low temperatures (200–300 °C) compared to conventional oxide-ion conductors such as YSZ.[140]

3.5 Nanomaterials and heterostructures

A broad area that is attracting increasing attention is nano-structured materials and "nano-ionics". These systems are characterised by size effects, short diffusion lengths, a high density of interfaces (*e.g.*, grain boundaries), and, in some cases, enhanced transport properties. More detailed discussions are found in reviews by Maier,[141] Chadwick and Savin[142] and Arico *et al.*[143]

Synthesis of bulk nanostructured materials has been made possible through the development of new sintering procedures such as spark plasma sintering (SPS), which allows the preparation of fully dense compacts while limiting grain growth. With this method it is possible to produce fully dense ceria pellets with grain diameters 15 nm or less.[144] Such materials show reasonable proton conductivity from room temperature to about 200 °C, depending on the water partial pressure.[145] This represents an increase of up to four orders of magnitude relative to samples with micron-sized grains. Such nanostructured electrolytes have been used in water concentration cells to generate power at room temperature.[146]

Garcia-Barriocanal *et al.*[147] reported an eight-orders-of-magnitude enhancement of YSZ conductivity in epitaxial heterostructures consisting of two-unit-cell thick YSZ thin films sandwiched between two thicker layers of strontium titanate ($SrTiO_3$, STO). A representation of the YSZ/STO interface is shown in Fig. 13. The origin of this huge enhancement in conductivity and associated decrease in activation energy (from 1.1 to 0.6 eV) is thought to lie in the YSZ/STO interfaces, in which the number of mobile ions increases, as does the volume through which they can move. This interface has been investigated by means of energy-loss spectroscopy, showing that epitaxial growth between YSZ and STO leads to a modified interface with a highly disordered oxygen plane.

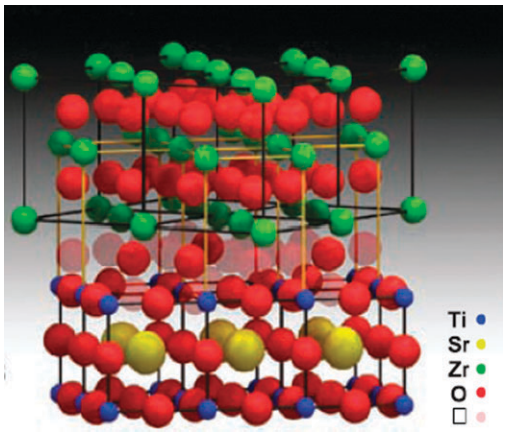

Fig. 13 Schematic of the YSZ/STO interface (ion radii are not to scale). The transparent O atoms represent empty sites, □, available for oxide ions at the interface. Reprinted with permission from ref. 147, copyright Science, 2008.

It has been suggested that the combination of the large number of mobile ions together with the expansion of the fluorite structure imposed by the substrate is the origin of the high interfacial conductivity.[148] However, these results have still to be independently verified, as there is some debate as to whether the conductivity of these heterostructures is purely ionic.[148] Improved conductivities have also been measured for alternating layers of ceria and zirconia on alumina substrates.[149] In the case of nanocrystalline YSZ deposited on Mg substrates, in contrast, a drastic decrease in conductivity has been reported.[150] In any case, these kinds of novel processing strategies could lead to exciting new technologies based on nanostructured low-temperature oxide-ion conductors, and thus represent a potentially fruitful avenue of research.

4 Conventional proton conductors

Proton conductors can be classified into several categories either on the basis of the type of transport species, or, as is more common, on their working temperature. In this section we describe recent research on high-temperature solid-state proton conductors, which can be used as solid protonic electrolytes in SOFCs (Fig. 1(b)).[4,151] In general, these materials are all oxides.

4.1 Perovskite-structured oxides

The first report of high-temperature proton conductivity in an oxide material dates back to the 1980s when Iwahara and co-workers observed this phenomenon in doped strontium and barium cerates.[152–153] After more than 20 years of active research, the perovskite-type cerates and zirconates have become well-established proton conducting systems.[154–159] The crystal structures of these materials are based on the perovskite structure, illustrated in Fig. 4. Protonic defects are

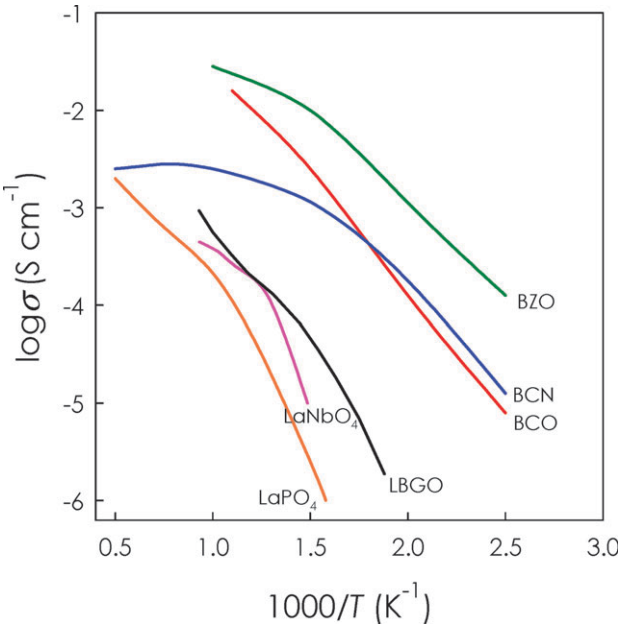

Fig. 14 Total conductivities of some well-known proton conductors as a function of inverse temperature: $BaCe_{0.9}Y_{0.1}O_3$ (BCO);[160] $BaZr_{0.8}Y_{0.2}O_3$ (BZO);[160] $La_{0.9}Sr_{0.1}PO_4$;[203] $Ba_3Ca_{1.18}Nb_{1.82}O_{8.73}$ (BCN);[189] $La_{0.99}Ca_{0.01}NbO_4$;[208] $La_{0.8}Ba_{1.2}GaO_{3.9}$ (LBGO).[115]

formed by the dissociative absorption of water at the surface, which requires the presence of oxide-ion vacancies. Water from the gas-phase dissociates into a hydroxide ion and a proton, with the hydroxide ion filling an oxide-ion vacancy and the proton forming a covalent bond with a lattice oxygen. In Kröger-Vink notation, this reaction can be written

$$H_2O_{(g)} + V_O^{\bullet\bullet} + O_O^{\times} \rightarrow 2OH_O^{\bullet} \qquad (4)$$

Pure $SrCeO_3$, $BaCeO_3$, $CaZrO_3$ and $SrZrO_3$ exhibit only low proton incorporation unless doped with subvalent cations. In the $BaCeO_3$ system, for example, replacing Ce^{4+} ions with M^{3+} cations (typically Y^{3+}) is charge-compensated by formation of an oxygen vacancy:

$$2Ce_{Ce}^{\times} + M_2O_3 + O_O^{\times} \rightarrow 2M_{Ce}^{'} + V_O^{\bullet\bullet} + 2CeO_2 \qquad (5)$$

The energy of water incorporation in such systems has been found (both experimentally and theoretically) to be exothermic for doped and undoped cerates and zirconates,[57,160,161] which is consistent with the observation that proton uptake in perovskite oxides increases with decreasing temperature. Furthermore, incorporation of water in doped systems is more exothermic than in undoped systems. A typical conductivity *vs.* inverse temperature curve for 10 mol% Y-doped $BaCeO_3$ is shown in Fig. 14 together with other proton conductors discussed in this review.

Detailed characterisation of the structures of many cerates as a function of temperature and dopant concentration has been reported.[162–169] For example, in the case of $BaCe_{0.80}Y_{0.20}O_{2.9}$ (the cerate with the best performance observed so far) high-temperature neutron diffraction has revealed rich structural phase behaviour as a function of temperature. The crystal structure changes from monoclinic at room temperature, to orthorhombic at 500 °C, followed by

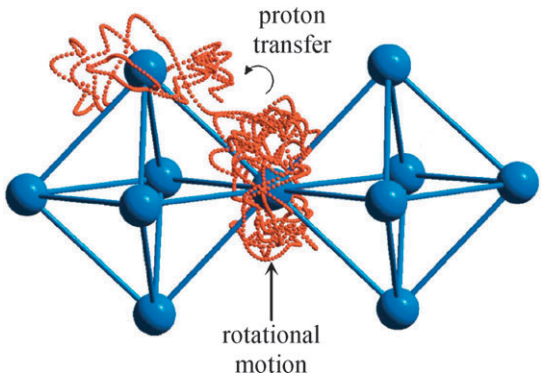

Fig. 15 Trace of a proton (orange) in $BaCeO_3$ showing the two main features of proton transport: rotational motion and proton transfer. Reprinted with permission from ref. 170, copyright Elsevier, 1996.

rhombohedral between 600 to 700 °C, finally assuming cubic symmetry at 800 °C.[166]

Quantum MD simulations of these perovskite systems have shown that proton transport involves hopping of a lone proton between oxide ions (the so-called Grotthuss mechanism), as well as rotational motion of the hydroxyl unit. This mechanism is illustrated in Fig. 15.[170] Computer simulations and experiments both confirm that the rate-limiting step is the proton-transfer between oxide ions, while the rotational motion is fast, with a low activation barrier.[170–175]

Any reduction in symmetry relative to the cubic structure is detrimental to the proton conductivity.[176] For example, the single crystallographic anion site in the cubic structure degenerates into two distinct sites with different energy levels in orthorhombic $SrCeO_3$.[176] The increased activation energy for proton transfer in the orthorhombic cerates can be attributed to these energetically different oxygen sites, which present an uneven energy hypersurface for the proton to travel across, as well as biasing the rotational diffusion (defect reorientation) to certain directions. Quantum MD simulations of the orthorhombic $CaZrO_3$ system,[177] for example, revealed a lower energy barrier between closely separated oxide ions of two tilting octahedra than in the other directions.

Dopant–hydroxyl group association is another issue to be considered in proton-conducting perovskites. Neutron-spin-echo experiments[178] on hydrated $BaZr_{1-x}Y_xO_{3-\delta}$ indicate trapping effects in which the proton spends an extended time in the vicinity of the Y dopant before further proton diffusion, confirming previous simulation predictions[175] and quasi-elastic neutron scattering (QENS) measurements.[174] In addition, "ambi-site" dopant behaviour in systems such as $BaCeO_3$ has also been observed, in which the site-occupancy of dopants is sensitive to barium loss. Certain cations (*e.g.*, Nd) show significant partitioning over both Ba and Ce sites in barium cerate.[179]

Despite intensive study, the main drawback in the use of barium cerates is that they have poor chemical stability and electronic species are formed under reducing conditions. In particular, in hydrocarbon- or syngas-fueled SOFCs below 800 °C, these materials react readily with CO_2, decomposing into barium carbonate and cerium oxide.[180] The chemical stability of doped barium zirconates is far greater.[181] Although

there is high intrinsic proton mobility in $BaZrO_3$, which is cubic at room temperature,[182] the conductivity of polycrystalline samples is often significantly lower than the bulk because of large grain boundary resistance.

In the case of $BaZr_{1-x}Y_xO_3$, samples often have low densities and poor conductivities, despite the use of high sintering temperatures (>1600 °C) or sintering additives.[183,184] Secondary phases, such as Y_2O_3, also segregate to the grain boundaries.[181] As a result, the conductivity of doped $BaZrO_3$ varies widely. Barium deficiency is the likely culprit for such inconsistent results, since exposure of the material to elevated temperatures for a prolonged time induces BaO vaporisation.

Perovskite cerates and zirconates are mutually soluble, so to develop electrolytes with adequate proton conductivity and good chemical stability under conditions typically encountered during fuel cell operation, cerate–zirconate solid solutions are being investigated.[181,184–187] Proton conducting cerates and zirconates thus represent one of the most promising and actively investigated groups of solid electrolytes. In addition to novel co-doping schemes for optimising conductivity and stability,[188] research is now also focusing on the development of chemically compatible electrodes for use in SOFCs.

4.2 Perovskite-related oxides

Another strategy for achieving high proton conductivities is to synthesise cation-offstoichiometric perovskites. The charge imbalance caused by the cation non-stoichiometry is compensated by protons. One of the best-known materials of this kind is $Ba_3Ca_{1.18}Nb_{1.82}O_{8.73}$ (also known as BCN18). The amount of water uptake in BCN18 per equivalent perovskite unit is comparable to that found for the cerates and zirconates.[189,190]

Aliovalent cation doping is frequently used as a means of introducing high concentrations of oxygen vacancies to enable water incorporation. However, there are some classes of materials characterised by a disordered oxygen sublattice where, for specific combinations of metal ions, the oxygen sites are only partially filled in the stoichiometric composition. This is the case for perovskite-related compounds of general formulae $Me_4(Me_2'M_2^{5+})O_{11}[V_O]$ (elpasolite) and $Me_6M_2^{5+}O_{11}[V_O]$ (cryolite), where Me is an alkaline-earth, M^{5+} either Nb or Ta, and V_O an intrinsic oxygen vacancy. Typical examples include $Sr_{6-2x}Nb_{2+2x}O_{11+3x}$, $Sr_{6-2x}Ta_{2+2x}O_{11+3x}$, and $(Ba_{1-y}Ca_y)_6Nb_2O_{11}$.[191,192] These phases are able to incorporate up to one water molecule per formula unit. In addition, for temperatures up to about 600 °C, the conductivities are purely protonic, although the values are relatively low (generally less than 10^{-3} S cm^{-1}).

$Ba_2In_2O_5$ is another perovskite-related oxygen deficient material. Initially proposed as an oxide-ion conductor,[193] its ability to conduct protons has also come under scrutiny.[194–198] The brownmillerite structure can be viewed as a perovskite-type structure in which one sixth of the oxide ions are missing. At room temperature, the oxygen vacancies order in alternating perovskite layers, so that the associated trivalent (B-site) cations exist in both tetrahedral and octahedral coordination, resulting in orthorhombic symmetry.[199] This ordering effectively traps the vacancies, preventing rapid ion conduction. Above ~900 °C, however, the oxide-ion conductivity abruptly increases, achieving values in excess of that of YSZ.[193,199] The high-conductivity phase can be stabilised to lower temperatures by partially replacing either Ba or In (or both).[200]

The presence of intrinsic oxygen vacancies in the structure means that it can also support significant proton conductivity. Investigations on the $(Ba_{1-x}La_x)_2In_2O_{5+x}$ system have shown that proton conduction increases with La content, with a maximum conductivity value of 1.12×10^{-5} S cm^{-1} for $x = 0.10$ at 400 °C.[201] Promising results have also been recently reported for the $Ba_2(In_{1-x}Ti_x)_2O_{5+x}$ system.[202] Conductivity measurements in dry and wet N_2 show that the highest level of proton conductivity, obtained for $x = 0.2$, is 1.1×10^{-3} S cm^{-1} at 450 °C for a very low level of hydration.[202] Investigations of these systems have begun relatively recently, and thus offer substantial opportunities for developing superior proton conductors.

4.3 Other related materials

Phosphates. Other high-temperature proton conductors receiving attention include phosphates without structural protons, such as $LaPO_4$. This compound was proposed as a candidate proton conductor in the early 1990s, and is interesting because of its unusual dissolution and proton transport mechanisms.[151] Ca- and Sr-doped $LaPO_4$ have been demonstrated to exhibit predominantly protonic conductivity up to ~800 °C, but with relatively low absolute conductivity values of 6×10^{-5} S cm^{-1} and 3×10^{-4} S cm^{-1}, respectively.[203,204] In these materials, protons are thought to enter the crystal from ambient water vapour in the form of extrinsic positive defects, compensating the acceptor dopants and replacing the intrinsic positive defects, presumably oxygen vacancies in the form of pyrophosphate groups.[203]

Detailed investigations of acceptor-doped $LaPO_4$ have revealed limited solubilities for the dopant ions. Excess doping leads to formation of secondary phases and strong segregation of dopants to the grain boundaries. For these reasons other phosphates have been attracting attention, such as lanthanum polyphosphate (or metaphosphate), LaP_3O_9,[205] and lanthanum oxophosphate, $La_7P_3O_{18}$.[206] Both of these compounds also exhibit protonic conduction in humid atmospheres when La is partially replaced with Sr, *e.g.*, 3×10^{-4} S cm^{-1} at 700 °C, which is comparable to some perovskite-type high-temperature protonic conductors such as In-doped $CaZrO_3$.[203] In all these phosphate systems, the structure consists of chains of corner-sharing PO_4 tetrahedra separated by layers containing the rare earth.

Solid acids. Other inorganic solids showing high proton conductivities at moderate temperatures (120–300 °C) are solid acid compounds such as $CsHSO_4$ and CsH_2PO_4.[5,151,207] Their structures are usually comprised of oxyanions, XO_4, such as SO_4 or PO_4, linked together by hydrogen bonds. Unlike the polymers in PEM fuel cells, the proton migration process is analogous to that found in the perovskites, with the protons hopping to a neighbouring tetrahedral oxygen, assisted by, for example, rapid phosphate group reorientation in the superprotonic disordered phase of CsH_2PO_4.[5] For fuel cell applications in vehicles, solid-acid electrolytes offer the

advantages of anhydrous proton transport and thermal stability (up to 250 °C). Continuous, stable power generation for both H_2/O_2 and direct methanol fuel cells using a humidity-stabilised electrolyte based on the solid acid CsH_2PO_4 has been demonstrated.[207]

5. New proton conductors

Although research into proton conducting oxides began more recently than oxide-ion conductors, several materials from the systems described above have been identified that display sufficient proton conductivity to be suitable for use in intermediate temperature SOFCs. In this section we describe some new materials systems that are being examined in the search for better high-temperature proton conducting solids.

5.1 Niobates and tantalates

While searching for more stable proton conducting materials, Norby and co-workers[208] came across several acceptor-doped rare-earth orthoniobates and orthotantalates of general formula $RE_{1-x}A_xMO_4$ (where RE = La, Gd, Nd, Tb, Er or Y; M = Nb or Ta; A = Ca, Sr or Ba; and x = 0.01–0.05). This class of materials crystallizes in the monoclinic fergusonite-type structure (space group $I2/c$) at low temperatures and in a tetragonal scheelite-type structure (space group $I4_1/a$) at high temperatures, with a transition temperature that varies with the chemical composition.[208]

The monoclinic and tetragonal structures are illustrated in Fig. 16, showing that both polymorphs contain isolated tetrahedral units, which represent a new structural type for proton-conducting oxides. Unlike perovskite-type proton conductors, the highest conductivities in the niobates and tantalates are obtained for relatively low doping levels, on the order of a few mole percent. As with other systems, acceptor doping is necessary to create high concentrations of oxygen vacancies.

Of the compositions investigated so far, $La_{0.99}Ca_{0.01}NbO_{4-\delta}$ has been reported to have the highest conductivity (shown in Fig. 14). In general, La-containing niobates are found to have higher proton mobilities than other RE-containing phases, consistent with their larger lattice volumes.

The two different polymorphs, the fergusonite-type and scheelite-type, have different activation energies for proton migration: 0.73–0.83 eV in the former and 0.52–0.62 eV in the latter, depending on the composition.[208,209] In general, the transition temperature increases with decreasing rare-earth cation size within the temperature range 500–830 °C for the niobates and considerably higher for the isostructural tantalates (1300–1450 °C). Neutron diffraction of $La_{0.99}Ca_{0.01}NbO_{4-\delta}$ at high temperature has shown that this phase change occurs without an abrupt volume change, which is a positive feature when considering its application inside any kind of practical device.[210]

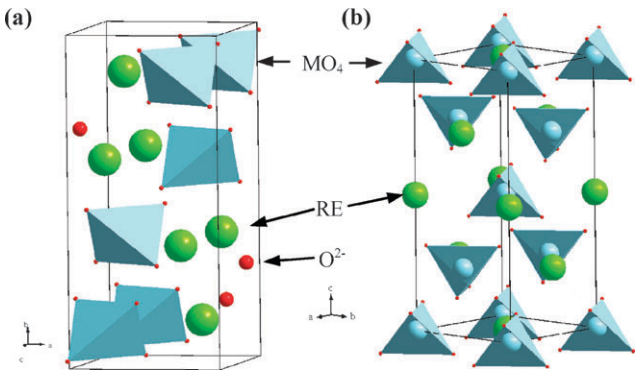

Fig. 16 Structures of orthoniobates and orthotantalates $REMO_4$ (where RE = rare earth and M = Nb or Ta); (a) monoclinic (b) tetragonal.

Transport number measurements for various niobates and tantalates indicate that the conductivity of these materials is fully protonic for temperatures up to 700 °C; at higher temperatures, the proton concentration decreases and positively charged native point defects, most likely oxygen vacancies, become the dominant mobile species.[208,209,211,212] Conductivity values measured for optimally doped niobates, which are of the order of 10^{-3} S cm^{-1}, suggest that a fuel cell containing an electrolyte a few microns thick may achieve reasonable area-specific power densities.[208]

The proton conduction mechanism in niobates and tantalates has only recently been investigated, both experimentally and theoretically. Density functional theory (DFT) based calculations on the tetragonal $LaNbO_4$ phase indicate that oxygen vacancies in the structure lead to formation of complex polyhedra.[213] Such a phenomenon is very similar to that observed in the $LaPO_4$ system, where $P_2O_7^{4-}$ replaces two PO_4^{3-} polyhedra in the Sr-doped sample under dry conditions,[213,214] as well as in the $La_{1-x}Ba_{1+x}GaO_{4-x/2}$ system, in which corner-sharing Ga_2O_7 units form.[114] Similarly in $LaNbO_4$ removal of an oxide ion from a tetrahedrally coordinated cation is compensated by local condensation of the tetrahedra to form larger linkages of $Nb_2O_7^{4-}$ or $Nb_3O_{11}^{7-}$ polyhedra.[213]

Recent tests have used Sr-doped $LaNbO_4$ as an electrolyte within a fuel cell with $NiO/LaNbO_4$ as the anode and different cathode materials, such as $CaTi_{0.9}Fe_{0.1}O_{3-\delta}$, La_2NiO_4 and $La_4Ni_3O_{10}$.[215] The $CaTi_{0.9}Fe_{0.1}O_{3-\delta}$ monophase cathode and $LaNbO_4/La_4Ni_3O_{10}$ composite anode showed good adhesion and no interfacial reaction with the electrolyte.

Even though the conductivities of these materials are lower than those of the perovskite-type cerates, they show the highest levels of proton conductivity reported so far for oxides not containing Ba or Sr as the main component. They thus represent a promising family of materials for use as thin-film electrolytes for SOFCs capable of operating in CO_2-containing atmospheres.

5.2 Gallium-based oxides

Other materials containing tetrahedral units that exhibit high temperature proton conductivity include lanthanum gallates of general formula $La_{1-x}Ba_{1+x}GaO_{4-x/2}$.[114–116] The rapid oxide-ion conductivity of this system was described in Section 3.3; in fact, its proton conductivity is even more significant. Typical proton conductivities reported for the composition $La_{0.8}Ba_{1.2}GaO_{3.9}$ are included in Fig. 14. The proton conductivities of these gallate-based compounds are among the highest measured at intermediate temperatures of all systems containing four-coordinate cation groups, exceeding, for example, that of Sr-doped $LaPO_4$.[114,115]

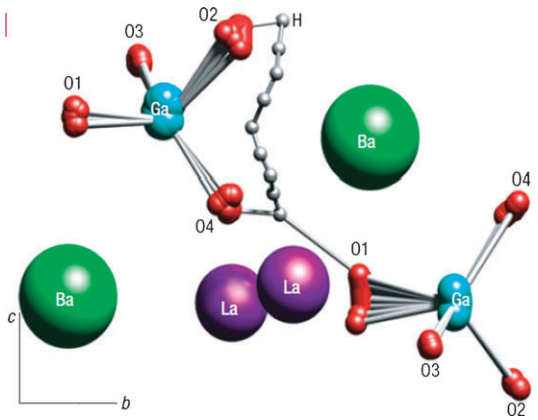

Fig. 17 Calculated proton migration pathway in $LaBaGaO_4$[112] as a composite of snapshots of H (grey). This indicates fast inter-tetrahedra migration (O1 to O4), and higher energy barrier intra-tetrahedra migration (O4 to O2). There is significant local ion movement, with the O–O separation contracting to about 2.5 Å to facilitate proton transfer.

Possible locations for the proton within the $La_{1-x}Ba_{1+x}GaO_{4-x/2}$ structure and its migration path have been examined using potential-based and density functional theory (DFT) calculations.[114] The calculated energy for water incorporation, around −0.60 eV, is comparable to the exothermic values obtained experimentally for other proton conducting oxides.[160,161,216] The simulations suggest that the rate-determining step for long-range proton diffusion is the intra-tetrahedral migration (as illustrated in Fig. 17). The calculated energy barrier for such a process is around 0.75 eV, which is in excellent agreement with an experimentally measured activation energy of 0.76 eV.[116,217] Proton diffusion is also calculated to be isotropic; in other words, the H-bonding-mediated transfer of protons between GaO_4 units within a layer and between layers is equally favourable.[114] Further work, including additional doping studies, is required to optimise the proton conductivity in this system.

6. Conclusions and future outlook

This review has highlighted the diverse classes of oxide materials exhibiting fast oxide-ion or proton conductivity, particularly for use as electrolytes in solid oxide fuel cells. In addition to describing conventional ion conductors such as fluorite oxides (*e.g.*, YSZ and CGO) and perovskite oxides (*e.g.*, Mg/Sr-doped $LaGaO_3$ and Y-doped $BaZrO_3$), new candidate materials and alternative structure types have been described. These include oxide-ion conductors based on $La_2Mo_2O_9$, Si/Ge apatites (*e.g.*, $La_{9.33+x}(Si/GeO_4)_6O_{2+3x/2}$), and gallates (*e.g.*, $LaSrGa_3O_7$), and proton conductors based on niobates (*e.g.*, Ca-doped $LaNbO_4$) and gallates (*e.g.*, $LaBaGaO_4$).

The structures of many of these new ion conductors consist of tetrahedral frameworks. Flexibility and ease of deformation of the tetrahedral units appears to be key to the ion conduction mechanisms. In many cases, deeper atomic-scale insights into the local structures, the defect types (oxygen vacancy, oxygen interstitial or protonic) and the transport mechanisms have been achieved through a combination of experimental and computer modelling techniques. Of particular note is the emergence of Si/Ge apatite-based oxide-ion conductors in which interstitial oxide-ion defects (rather than vacancies as in YSZ) play a critical role.

In addition to the major issues covered in this review, future studies are likely to encompass the following key areas:

(i) Materials optimisation

There are still many strategies to explore to further optimise both new and conventional electrolyte materials (especially for reducing SOFC costs by lowering operating temperatures). These strategies include chemical doping, novel synthesis/processing routes and dense thin film preparation. Technical challenges to be addressed include mechanical stability and cell/stack durability.

(ii) Materials discovery

There will be continuing efforts to explore new compounds that support fast oxide-ion or proton conductivity particularly in systems containing flexible tetrahedral networks. The Si/Ge apatites and melilite gallates have shown that introduction of interstitial defects can profoundly alter the electrochemical behaviour. Similar strategies should be attempted for other structure types in the search for novel interstitial oxide-ion conductors.

(iii) Nanostructured materials

Nanostructured multi-layers with heterogeneous oxide interfaces will continue to make inroads in the production of new materials, where interfacial strain is believed to play a critical role. A better understanding is required of "nano-ionics", and the effects of a high density of interfaces and short diffusion lengths on materials properties.

(iv) Materials characterisation

In addition to crystallographic studies of the average structure, there will be increasing use of atomic-scale characterisation and computer modelling techniques to probe local and nano-level structures, ion conduction mechanisms and interface chemistry. Such techniques will encompass *in situ* synchrotron XRD, ^{17}O NMR, and pair distribution function (PDF) analysis and maximum entropy methods (MEM) using diffraction data.

In conclusion, though considerable progress has been made in the development of fuel cell technology, it is clear that future advances still depend on exploring novel compounds and structure types, and on a greater fundamental understanding of the structural, defect and mechanistic features of ion conducting materials.

Acknowledgements

The authors are grateful to the EPSRC and the INSTM-Regione Lombardia Project "PICASSO" for financial support, and to P. R. Slater, E. Kendrick, C. Tealdi, G. Gardiner and P. Panchmatia for useful discussions.

Notes and references

1 B. C. H. Steele and A. Heinzel, *Nature*, 2001, **414**, 345; J. B. Goodenough, *Annu. Rev. Mater. Res.*, 2003, **33**, 91; S. M. Haile, *Acta Mater.*, 2003, **51**, 5981.
2 D. J. L. Brett, A. Atkinson, N. P. Brandon and S. J. Skinner, *Chem. Soc. Rev.*, 2008, **37**, 1568; A. Orera and P. R. Slater, *Chem. Mater.*, 2010, **22**, 675; A. J. Jacobson, *Chem. Mater.*, 2010, **22**, 660; J. A. Kilner, *Faraday Discuss.*, 2007, **134**, 9; V. V. Kharton, F. M. B. Marques and A. Atkinson, *Solid State Ionics*, 2004, **174**, 135; H. L. Tuller, *Phys. Chem. Chem. Phys.*, 2009, **11**, 3023; N. Q. Minh, *Solid State Ionics*, 2004, **174**, 271; ref. 59.
3 O. H. Kwon and G. M. Choi, *Solid State Ionics*, 2006, **177**, 3057.
4 K. D. Kreuer, *J. Membr. Sci.*, 2001, **185**, 29; V. Neburchilov, J. Martin, H. J. Wang and J. J. Wang, *J. Power Sources*, 2007, **169**, 221.
5 S. Haile, C. R. I. Chisholm, K. Sasaki, D. A. Boysen and T. Uda, *Faraday Discuss.*, 2007, **134**, 17.
6 H. G. Scott, *J. Mater. Sci.*, 1975, **10**, 1527.
7 A. W. Smith, F. W. Meszaros and C. D. Kamata, *J. Am. Ceram. Soc.*, 1996, **9**, 240.
8 K. Kitazawa and R. L. Coble, *J. Am. Ceram. Soc.*, 1974, **57**, 360.
9 L. D. Burke, H. Rickert and R. Steiner, *Z. Phys. Chem., N. F.*, 1971, **74**, 146.
10 T. Kawada and J. Mizusaki, in *Handbook of Fuel Cells—Fundamentals, Technology and Applications*, ed. W. Vielstich, H. A. Gasteiger and A. Lamm, John Wiley Sons, New Jersey, USA, 2003, vol. 4, pp. 987–1001; S. Q. Hui, J. Roller, S. Yick, X. Zhang, C. Deces-Petit, Y. S. Xie, R. Maric and D. Ghosh, *J. Power Sources*, 2007, **172**, 493; X. Guo and R. Waser, *Prog. Mater. Sci.*, 2006, **51**, 151.
11 T. I.. Politova and J. T. S. Irvine, *Solid State Ionics*, 2004, **168**, 153.
12 A. Lashtabeg and S. J. Skinner, *J. Mater. Chem.*, 2006, **16**, 3161.
13 S. P. S. Badwal, F. T. Ciacchi and D. Milosevic, *Solid State Ionics*, 2000, **136–137**, 91; S. Sarat, N. Sammes and A. Smirnova, *J. Power Sources*, 2006, **160**, 892; R. Devanathan, S. Thevuthasan and J. D. Gale, *Phys. Chem. Chem. Phys.*, 2009, **11**, 5506.
14 K. Eguchi, T. Setoguchi, T. Inoue and H. Arai, *Solid State Ionics*, 1992, **52**, 165; H. L. Tuller and A. S. Nowick, *J. Electrochem. Soc.*, 1975, **122**, 255; J. A. Kilner, *Chem. Lett.*, 2008, **37**, 1012; M. Mogensen, N. M. Sammes and G. A. Tompsett, *Solid State Ionics*, 2000, **129**, 63; M. Mogensen, D. Lybye, N. Bonanos, P. V. Hendriksen and F. W. Poulsen, *Solid State Ionics*, 2004, **174**, 279; T. Inoue, T. Setoguchi, K. Eguchi and H. Arai, *Solid State Ionics*, 1989, **35**, 285.
15 O. A. Marina, C. Bagger, S. Primdahl and M. Mogensen, *Solid State Ionics*, 1999, **123**, 199; H. J. Avila, P. Jain, S. Sen and S. Kim, *Chem. Mater.*, 2010, **22**, 893.
16 B. C. H. Steele, *Solid State Ionics*, 2000, **129**, 95.
17 K. Zheng, B. C. H. Steele, M. Sahibzada and I. S. Metcalfe, *Solid State Ionics*, 1996, **86–88**, 1241.
18 M. Sahibzada, B. C. H. Steele, K. Zheng, R. A. Rudkin and I. S. Metcalfe, *Catal. Today*, 1997, **38**, 459.
19 H. Inaba and H. Tagawa, *Solid State Ionics*, 1996, **83**, 1.
20 S. Wang, H. Inaba, H. Tagawa, M. Dokiya and T. Hashimoto, *Solid State Ionics*, 1998, **107**, 73.
21 V. V. Kharton, F. M. Figueiredo, L. Navarro, E. N. Naumovich, A. V. Kovalevsky, A. A. Yaremchenko, A. P. Viskup, A. Carniero, F. M. B. Marques and J. R. Frade, *J. Mater. Sci.*, 2001, **36**, 1105.
22 S. Omar, E. D. Wachsman and J. C. Nino, *Solid State Ionics*, 2008, **178**, 1890.
23 T. Kudo and H. Obayashi, *J. Electrochem. Soc.*, 1976, **123**, 415; C. Milliken, S. Guruswamy and A. Khandkar, *J. Am. Ceram. Soc.*, 2002, **85**, 2479.
24 A. Guesdon, Y. Monnin and B. Raveau, *J. Solid State Chem.*, 2003, **172**, 237.
25 D. J. Seo, K. O. Ryu, S. B. Park, K. Y. Kim and R.-H. Song, *Mater. Res. Bull.*, 2006, **41**, 359.
26 V. Butler, C. R. A. Catlow and B. E. F. Fender, *Solid State Ionics*, 1983, **8**, 109; L. Minervini, M. O. Zacate and R. W. Grimes, *Solid State Ionics*, 1999, **116**, 339.
27 D. Pérez-Coll and G. C. Mather, *Solid State Ionics*, 2010, **181**, 20.
28 D. Schneider, M. Gödickemeier and L. J. Gauckler, *J. Electroceram.*, 1997, **1**, 165.
29 J. A. Kilner, *Solid State Ionics*, 2000, **129**, 13.
30 S. Omar, E. D. Wachsman, J. L. Jones and J. C. Nino, *J. Am. Ceram. Soc.*, 2009, **92**, 2674.
31 T.-H. Yeh and C.-C. Chou, *Solid State Ionics*, 2009, **180**, 1529.
32 T. Takahashi, H. Iwahara and T. Arao, *J. Appl. Electrochem.*, 1975, **5**, 187; N. M. Sammes, G. A. Tompsett, H. Nafe and F. Aldinger, *J. Eur. Ceram. Soc.*, 1999, **19**, 1801.
33 H. J. M. Bouwmeester and A. J. Burggraaf, in *Fundamentals of Inorganic Membrane Science and Technology*, ed. A. Burggraaf and L. Cot, Elsevier, Amsterdam, 1996, p. 435.
34 A. A. Yaremchenko, V. V. Kharton, E. N. Naumovich, A. A. Tonoyan and V. V. Samokhval, *J. Solid State Electrochem.*, 1998, **2**, 308.
35 V. V. Kharton, E. N. Naumovich, A. A. Yaremchenko and F. M. B. Marques, *J. Solid State Electrochem.*, 2001, **5**, 160.
36 P. Shuk, H.-D. Wiemhofer, U. Guth, W. Gopel and M. Greenblatt, *Solid State Ionics*, 1996, **89**, 179.
37 P. D. Battle, G. Hu, L. M. Moroney and D. C. Munro, *J. Solid State Chem.*, 1987, **69**, 30; A. Watanabe, *Solid State Ionics*, 2005, **176**, 2423; H. Kruidhof, H. J. M. Bouwmeester, K. J. Devries, P. J. Gellings and A. J. Burggraaf, *Solid State Ionics*, 1992, **50**, 181.
38 N. Jiang, E. D. Wachsman and S. Jung, *Solid State Ionics*, 2002, **150**, 347.
39 K. R. Kendall, J. K. Thomas and H.-C. zur Loye, *Solid State Ionics*, 1994, **70–71**, 221.
40 R. Punn, A. M. Feteira, D. C. Sinclair and C. Greaves, *J. Am. Chem. Soc.*, 2006, **128**, 15386.
41 S. Hull, S. T. Norberg, M. G. Tucker, S. G. Eriksson, C. E. Mohn and S. Stølen, *Dalton Trans.*, 2009, 8737; C. E. Mohn, S. Stølen, S. T. Norberg and S. Hull, *Phys. Rev. Lett.*, 2009, **102**, 155502.
42 D. W. Jung, K. L. Duncan and E. D. Wachsman, *Acta Mater.*, 2010, **58**, 355; D. W. Jung, J. C. Nino, S. R. Bishop, K. L. Duncan and E. D. Wachsman, *Ionics*, 2010, **16**, 97.
43 H. L. Tuller, *Solid State Ionics*, 1992, **52**, 135.
44 T. H. Yu and H. L. Tuller, *J. Electroceram.*, 1998, **2**, 49.
45 J. A. Díaz-Guillén, M. R. Díaz-Guillén, K. P. Padmasree, A. F. Fuentes, J. Santamaría and C. León, *Solid State Ionics*, 2008, **179**, 2160.
46 T. Ishihara, H. Matsuda and Y. Takata, *J. Am. Chem. Soc.*, 1994, **116**, 3801.
47 M. Feng and J. B. Goodenough, *Eur. J. Solid State Inorg. Chem.*, 1994, **T31**, 663.
48 K. Huang, R. S. Tichy, J. B. Goodenough and C. Milliken, *J. Am. Ceram. Soc.*, 1998, **81**, 2581.
49 S. Tao, J. T. S. Irvine and J. A. Kilner, *Adv. Mater.*, 2005, **17**, 1734.
50 A. Matraszek, L. Singheiser, D. Kobertz, K. Hilpert, M. Miller, O. Schulz and M. Martin, *Solid State Ionics*, 2004, **166**, 343.
51 K. Huang, M. Feng and J. B. Goodenough, *J. Electrochem. Soc.*, 1997, **144**, 3620.
52 H. Boysen, M. Lerch, R. Gilles, B. Krimmer and D. M. Többens, *Appl. Phys. A: Mater. Sci. Process.*, 2002, **74**, s966; M. Lerch, H. Boysen and T. Hansen, *J. Phys. Chem. Solids*, 2001, **62**, 445; P. Slater, J. T. S. Irvine, T. Ishihara and Y. Takita, *J. Solid State Chem.*, 1998, **139**, 135.
53 M. Kajitani, M. Matsuda, A. Hoshikawa, S. Harjo, T. Kamiyama, T. Ishigaki, F. Izumi and M. Miyake, *Chem. Mater.*, 2005, **17**, 4235.
54 M. S. Khan, M. S. Islam and D. Bates, *J. Phys. Chem. B*, 1998, **102**, 3099; M. S. Islam and R. A. Davies, *J.Mater. Chem.*, 2004, **14**, 86.
55 A. Kuwabara and I. Tanaka, *J. Phys. Chem. B*, 2004, **108**, 9168.
56 M. Yashima, K. Nomura, H. Kageyama, Y. Miyazaki, N. Chitose and K. Adachi, *Chem. Phys. Lett.*, 2003, **380**, 391.
57 M. S. Islam, *J. Mater. Chem.*, 2000, **10**, 1027; M. S. Islam and P. R. Slater, *MRS Bull.*, 2009, **34**, 935.
58 S. Li and B. Bergman, *J. Eur. Ceram. Soc.*, 2009, **29**, 1139.
59 J. W. Fergus, *J. Power Sources*, 2006, **162**, 30.
60 T. Ishihara, T. Shibayama, H. Nishiguchi and Y. Takita, *J. Mater. Sci.*, 2001, **36**, 1125; T. Ishihara, T. Shibayama, S. Ishikawa, K. Hosoi, H. Nishiguchi and Y. Takita, *J. Eur. Ceram. Soc.*, 2004, **24**, 1329.

61 H. Zhong, H. Matsumoto, A. Toriyama and T. Ishihara, *J. Electrochem. Soc.*, 2009, **156**, B74.
62 T. Ishihara, H. Matsuda, M. Azmi Bin Bustam and Y. Takita, *Solid State Ionics*, 1996, **86–88**, 197; A. Petric and P. Huan, *Solid State Ionics*, 1996, **92**, 113.
63 A. Sinha, H. Näfe, B. P. Sharma and P. Gopalan, *J. Electrochem. Soc.*, 2008, **155**, B309.
64 N. Zhou, G. Chen, H. J. Zhang and C. Zhou, *Phys. B*, 2009, **404**, 4150; A. Chroneos, D. Parfitt, J. A. Kilner and R. W. Grimes, *J. Mater. Chem.*, 2010, **20**, 266; M. Yashima, M. Enoki, T. Wakita, R. Ali, Y. Matsushita, F. Izumi and T. Ishihara, *J. Am. Chem. Soc.*, 2008, **130**, 2762–2763; H. S. Kim and H. I. Yoo, *Phys. Chem. Chem. Phys.*, 2010, **12**, 4704.
65 P. Lacorre, F. Goutenoire, O. Bohnke, R. Retoux and Y. Laligant, *Nature*, 2000, **404**, 856; F. Goutenoire, O. Isnard, R. Retoux and P. Lacorre, *Chem. Mater.*, 2000, **12**, 2575.
66 C. Tealdi, G. Chiodelli, L. Malavasi and G. Flor, *J. Mater. Chem.*, 2004, **14**, 3553.
67 I. R. Evans, J. A. K. Howard and J. S. O. Evans, *Chem. Mater.*, 2005, **17**, 4074.
68 F. Goutenoire, O. Isnard, E. Suard, O. Bohnke, Y. Laligant, R. Retoux and P. Lacorre, *J. Mater. Chem.*, 2001, **11**, 119.
69 M. O'Keeffe and B. G. Hyde, *Struct. Bonding*, 1985, **61**, 77.
70 C. Tealdi, L. Malavasi, C. Ritter, G. Flor and G. Costa, *J. Solid State Chem.*, 2008, **181**, 603.
71 L. Malavasi, H. Kim, S. J. L. Billinge, Th. Proffen, C. Tealdi and G. Flor, *J. Am. Chem. Soc.*, 2007, **129**, 6903.
72 X. P. Wang and Q. F. Fang, *Phys. Rev. B: Condens. Matter Mater. Phys.*, 2002, **65**, 064304; Q. F. Fang, X. P. Wang, G. G. Zhang and Z. G. Yi, *J. Alloys Compd.*, 2003, **355**, 177; S. Georges, S. J. Skinner, P. Lacorre and M. C. Steil, *Dalton Trans.*, 2004, 3101.
73 S. Georges, F. Goutenoire, F. Altorfer, D. Sheptyakov, F. Fauth, E. Suard and P. Lacorre, *Solid State Ionics*, 2003, **161**, 231.
74 X. P. Wang, Z. J. Cheng and Q. F. Fang, *Solid State Ionics*, 2005, **176**, 761.
75 I. T. Weber, P. R. Baracho, F. Rangel, E. C. Paris and E. N. S. Muccillo, *Mater. Sci. Technol.*, 2009, **25**, 1346.
76 S. Georges, F. Goutenoire, O. Bohnke, M. C. Steil, S. J. Skinner, H.-D. Wiemhöfer and P. Lacorre, *J. New. Mater. Electrochem. Syst.*, 2004, **7**, 51.
77 T. Ishihara, J. A. Kilner, M. Honda, N. Sakai, H. Yokokawa and Y. Takita, *Solid State Ionics*, 1998, **113–115**, 593.
78 F. Goutenoire, R. Retoux, E. Suard and P. Lacorre, *J. Solid State Chem.*, 1999, **142**, 228.
79 S. Georges, F. Goutenoire, Y. Laligant and P. Lacorre, *J. Mater. Chem.*, 2003, **13**, 2317.
80 D. Marrero-Lopez, J. Canales-Vazquez, J. C. Ruiz-Morales, J. T. S. Irvine and P. Nunez, *Electrochim. Acta*, 2005, **50**, 4385.
81 J. A. Collado, M. A. G. Aranda, A. Cabeza and P. Olivera-Pastor, *J. Solid State Chem.*, 2002, **167**, 80.
82 D. Marrero-López, J. Pena-Martinez, J. C. Ruiz-Morales and P. Nunez, *J. Solid State Chem.*, 2008, **181**, 253.
83 P. Pinet and J. Fouletier, *Mater. Res. Bull.*, 2007, **42**, 935.
84 S. Nakayama, H. Aono and Y. Sadaoka, *Chem. Lett.*, 1995, 431.
85 S. Nakayama, T. Kagayama, H. Aono and Y. Sadoaka, *J. Mater. Chem.*, 1995, **5**, 1801.
86 E. Kendrick, M. S. Islam and P. R. Slater, *J. Mater. Chem.*, 2007, **17**, 3104.
87 S. Nakayama, Y. Higuchi, Y. Kondo and M. Sakamoto, *Solid State Ionics*, 2004, **170**, 219; H. Zhang, F. Li, J. Jin, Q. Wang and Y. Sun, *Solid State Ionics*, 2008, **179**, 1024.
88 L. León-Reina, E. R. Losilla, M. Martinez-Lara, S. Bruque and M. A. G. Aranda, *J. Mater. Chem.*, 2004, **14**, 1142; V. V. Kharton, A. L. Shaula, M. V. Patrakeev, J. C. Waerenborgh, D. P. Rojas, N. P. Vyshatko, E. V. Tsipis, A. A. Yaremchenko and F. M. B. Marques, *J. Electrochem. Soc.*, 2004, **151**, A1236.
89 M. Higuchi, Y. Masubuchi, S. Nakayama, S. Kikkawa and K. Kodaira, *Solid State Ionics*, 2004, **174**, 73.
90 J. E. H. Sansom, D. Richings and P. R. Slater, *Solid State Ionics*, 2001, **139**, 205.
91 A. Najib, J. E. H. Sansom, J. R. Tolchard, P. R. Slater and M. S. Islam, *Dalton Trans.*, 2004, 3106.
92 J. McFarlane, S. Barth, M. Swaffer, J. E. H. Sansom and P. R. Slater, *Ionics*, 2002, **8**, 149.
93 J. R. Tolchard, P. R. Slater and M. S. Islam, *Adv. Funct. Mater.*, 2007, **17**, 2564.
94 A. Al-Yasari, A. Jones, A. Orera, D. C. Apperley, D. Driscoll, M. S. Islam and P. R. Slater, *J. Mater. Chem.*, 2009, **19**, 5003.
95 S. S. Pramana, W. T. Klooster and T. J. White, *Acta Crystallogr., Sect. B: Struct. Sci.*, 2007, **63**, 597.
96 A. Orera, D. Headspith, D. C. Apperley, M. G. Francesconi and P. R. Slater, *J. Solid State Chem.*, 2009, **182**, 3294.
97 E. Kendrick and P. R. Slater, *Mater. Res. Bull.*, 2008, **43**, 2509; S. S. Pramana, W. T. Klooster and T. J. White, *J. Solid State Chem.*, 2008, **181**, 1717.
98 J. R. Tolchard, M. S. Islam and P. R. Slater, *J. Mater. Chem.*, 2003, **13**, 1956.
99 J. E. H. Sansom, J. R. Tolchard, D. Apperley, M. S. Islam and P. R. Slater, *J. Mater. Chem.*, 2006, **16**, 1410.
100 A. Orera, E. Kendrick, D. C. Apperley, V. M. Orera and P. R. Slater, *Dalton Trans.*, 2008, 5296; L. León-Reina, E. R. Losilla, M. Martínez-Lara, S. Bruque, A. Llobet, D. V. Sheptyakov and M. A. G. Aranda, *J. Mater. Chem.*, 2005, **15**, 2489.
101 R. Ali, M. Yashima, Y. Matsushita, H. Yoshioka and F. Izumi, *J. Solid State Chem.*, 2009, **182**, 2846.
102 E. Béchade, O. Masson, T. Iwata, I. Julien, K. Fukuda, P. Thomas and E. Champion, *Chem. Mater.*, 2009, **21**, 2508.
103 E. Kendrick, M. S. Islam and P. R. Slater, *Chem. Commun.*, 2008, 715.
104 E. Kendrick, A. Orera and P. R. Slater, *J. Mater. Chem.*, 2009, **19**, 7955.
105 L. León-Reina, J. M. Porras-Vasquez, E. R. Losilla and M. A. G. Aranda, *J. Solid State Chem.*, 2007, **180**, 1250.
106 A. Orera and P. R. Slater, *Solid State Ionics*, 2010, **181**, 110; P. M. Panchmatia, A. Orera, E. Kendrick, J. V. Hanna, M. E. Smith, P. R. Slater and M. S. Islam, *J. Mater. Chem.*, 2010, **20**, 2766.
107 S. H. Jo, P. Muralidharan and D. K. Kim, *J. Mater. Res.*, 2009, **24**, 237.
108 C. Tian, J. Liu, J. Cai and Y. Zeng, *J. Alloys Compd.*, 2008, **458**, 378.
109 E. Rodríguez-Reyna, A. F. Fuentes, M. Maczka, J. Hanuza, K. Boulahya and U. Amador, *J. Solid State Chem.*, 2006, **179**, 522.
110 C. Y. Ma, P. Briosis, J. Boehlmark, F. Lapostolle and A. Billard, *Ionics*, 2008, **14**, 471.
111 J. C. Oliveira, D. Horwat, A. Billard and A. Cavaleiro, *Thin Solid Films*, 2009, **517**, 1895.
112 A. L. Shaula, J. C. Oliveira, V. A. Kolotygin, C. Louro, V. V. Kharton and A. Cavaleiro, *Vacuum*, 2009, **83**, 1266.
113 D. Marrero-López, M. C. Martin-Sedeno, J. C. Ruiz-Morales, P. Nunez, M. A. G. Aranda and J. R. Ramos-Barrado, *J. Power Sources*, 2010, **195**, 2496; C. Bonhomme, S. Beaudet-Savignat, T. Chartier, C. Pirovano and R. N. Vannier, *Mater. Res. Bull.*, 2010, **45**, 491.
114 E. Kendrick, J. Kendrick, K. S. Knight, M. S. Islam and P. R. Slater, *Nat. Mater.*, 2007, **6**, 871.
115 S. Li, F. Schönberger and P. R. Slater, *Chem. Commun.*, 2003, 2694.
116 F. Schönberger, E. Kendrick, M. S. Islam and P. R. Slater, *Solid State Ionics*, 2005, **176**, 2951.
117 X. Kuang, M. A. Green, H. Niu, P. Zajdel, C. Dickinson, J. B. Claridge, L. Jantsky and M. J. Rosseinsky, *Nat. Mater.*, 2008, **7**, 498; C. I. Thomas, X. J. Kuang, Z. Q. Deng, H. J. Niu, J. B. Claridge and M. J. Rosseinsky, *Chem. Mater.*, 2010, **22**, 2510.
118 J. M. S. Skalke and R. Herd, *Powder Diffraction*, 1999, **14**, 195.
119 M. Rozumek, P. Majewski, L. Sauter and F. Aldinger, *J. Am. Ceram. Soc.*, 2004, **87**, 662; E. S. Raj, S. J. Skinner and J. A. Kilner, *Solid State Ionics*, 2005, **176**, 1097.
120 M. Rozumek, P. Majewski, H. Schluckwerder, F. Aldinger, K. Künstler and G. Tomandl, *J. Am. Ceram. Soc.*, 2004, **87**, 1795.
121 C. Tealdi, P. Mustarelli and M. S. Islam, *Adv. Funct. Mater.*, DOI: 10.1002/adfm.201001137.
122 M. Lacerda, J. T. S. Irvine, F. P. Glasser and A. R. West, *Nature*, 1988, **332**, 525.

123 H. Boysen, I. Kaiser-Bischoff and M. Lerch, *Diffusion Fundam.*, 2008, **8**, 2.1–2.8.
124 H. Hosono, K. Hayashi, K. Kajihara, P. V. Sushko and A. L. Shluger, *Solid State Ionics*, 2009, **180**, 550; R. Strandbakke, C. Kongshaug, R. Haugsrud and T. Norby, *J. Phys. Chem. C*, 2009, **113**, 8938; D.-K. Lee, L. Kogel, S. G. Ebbinghaus, I. Valov, H.-D. Wiemhoefer, M. Lerch and J. Janek, *Phys. Chem. Chem. Phys.*, 2009, **11**, 3105.
125 F. Abraham, M. F. Debreville-Gresse, G. Mairesse and G. Novogrocki, *Solid State Ionics*, 1988, **116**, 28.
126 I. Abrahams and F. Krok, *J. Mater. Chem.*, 2002, **12**, 3351.
127 J. C. Boivin and G. Mairesse, *Chem. Mater.*, 1998, **10**, 2870; M. C. Steil, J. Fouletier, M. Kleitz and P. Labrune, *J. Eur. Ceram. Soc.*, 1999, **19**, 815.
128 N. Kim and C. P. Grey, *Science*, 2002, **297**, 1317.
129 N. Kim, R. N. Vannier and C. P. Grey, *Chem. Mater.*, 2005, **17**, 1952.
130 R. N. Vannier, G. Mairesse, F. Abraham and G. Nowogrocki, *Solid State Ionics*, 1994, **70–71**, 248.
131 F. Krok, W. Bogusz, W. Jakubowski, J. R. Dygas and D. Bangobango, *Solid State Ionics*, 1994, **70–71**, 211; M. Malys, M. Holdynski, F. Krok, W. Wrobel, J. R. Dygas, C. Pirovano, R. N. Vannier, E. Capoen and I. Abrahams, *J. Power Sources*, 2009, **194**, 16.
132 Y. L. Yang, L. Qiu, W. T. A. Harrison, R. Christoffersen and A. J. Jacobson, *J. Mater. Chem.*, 1997, **7**, 243.
133 A. J. Francklin, A. V. Chadwick and J. W. Couves, *Solid State Ionics*, 1994, **70–71**, 215.
134 C. K. Lee, D. C. Sinclair and A. R. West, *Solid State Ionics*, 1993, **62**, 193.
135 J. C. Boivin, C. Pirovano, G. Nowogrocki, G. Mairesse, Ph. Labrune and G. Lagrange, *Solid State Ionics*, 1998, **113–115**, 639.
136 A. Watanabe and K. Das, *J. Solid State Chem.*, 2002, **163**, 224.
137 R. N. Vannier, R. J. Chater, S. J. Skinner, J. A. Kilner and G. Mairesse, *Solid State Ionics*, 2003, **160**, 327.
138 V. N. Tikhonovich, E. N. Naumovich, V. V. Kharton, A. A. Yaremchenko, A. V. Kovalevsky and A. A. Vecher, *Electrochim. Acta*, 2002, **47**, 3957.
139 B. Roy and P. A. Fuierer, *J. Am. Ceram. Soc.*, 2009, **92**, 520; S. Beg, N. A. S. Al-Areqi and S. Haneef, *Solid State Ionics*, 2008, **179**, 2260.
140 R. Karoum, C. Pirovano, R. N. Vannier, P. Vernoux and A. Billard, *Catal. Today*, 2009, **146**, 359.
141 J. Maier, *Nat. Mater.*, 2005, **4**, 805.
142 A. Chadwick and S. L. P. Savin, *Solid State Ionics*, 2006, **177**, 3001.
143 A. S. Aricò, P. Bruce, B. Scrosati, J.-M. Tarascon and W. van Schalkwijk, *Nat. Mater.*, 2005, **4**, 366.
144 U. Anselmi-Tamburini, F. Maglia, G. Chiodelli, A. Tacca, G. Spinolo, P. Riello, S. Bucella and Z. A. Munir, *Adv. Funct. Mater.*, 2006, **16**, 2363.
145 G. Chiodelli, F. Maglia, U. Anselmi-Tamburini and Z. A. Munir, *Solid State Ionics*, 2009, **180**, 297.
146 S. Kim, U. Anselmi-Tamburini, H. Jung Park, M. Martin and Z. A. Munir, *Adv. Mater.*, 2008, **20**, 556.
147 J. Garcia-Barriocanal, A. Rivera-Calzada, M. Varela, Z. Sefrioui, E. Iborra, C. Leon, S. J. Pennycook and J. Santamaria, *Science*, 2008, **321**, 676.
148 J. A. Kilner, *Nat. Mater.*, 2008, **7**, 838; X. Guo, *Science*, 2009, **324**, 5926; N. Schichtel, C. Kort, D. Hesse and J. Janek, *Phys. Chem. Chem. Phys.*, 2009, **11**, 3043.
149 Y. Wang, L. An, L. V. Saraf, C. M. Wang, V. Shutthanandan, D. E. McCready and S. Thevuthasan, *J. Mater. Sci.*, 2009, **44**, 2021.
150 X. Guo, E. Vasco, S. Mi, K. Szot, E. Wachsman and R. Waser, *Acta Mater.*, 2005, **53**, 5161.
151 T. Norby, *Solid State Ionics*, 1999, **125**, 1.
152 H. Iwahara, H. Uchida, K. Ono and K. Ogaki, *J. Electrochem. Soc.*, 1988, **135**, 529.
153 H. Iwahara, *Solid State Ionics*, 1988, **28–30**, 573.
154 T. Yajima, H. Kazeoka, T. Yogo and H. Iwahara, *Solid State Ionics*, 1991, **47**, 271.
155 T. Yajima, H. Suzuki, T. Yogo and H. Iwahara, *Solid State Ionics*, 1992, **51**, 101.
156 H. Iwahara, *Solid State Ionics*, 1992, **52**, 99.
157 H. Iwahara, T. Yajima, T. Hibino, K. Ozaki and H. Suzuki, *Solid State Ionics*, 1993, **61**, 65.
158 H. Iwahara, *Solid State Ionics*, 1996, **86–88**, 9–15.
159 K. Katahira, Y. Kohchi, T. Shimura and H. Iwahara, *Solid State Ionics*, 2000, **138**, 91.
160 K. D. Kreuer, *Annu. Rev. Mater. Res.*, 2003, **33**, 333.
161 T. Norby and Y. Larring, *Curr. Opin. Solid State Mater. Sci.*, 1997, **2**, 593; K. D. Kreuer, W. Münch, M. Ise, T. He, A. Fuchs, U. Traub and J. Maier, *Ber. Bunsenges. Phys. Chem.*, 1997, **101**, 1344.
162 K. S. Knight, *Solid State Ionics*, 2001, **145**, 275.
163 F. Genet, S. Loridant, C. Ritter and G. Lucazeau, *J. Phys. Chem. Solids*, 1999, **60**, 2009.
164 A. Kruth, R. A. Davies, M. S. Islam and J. T. S. Irvine, *Chem. Mater.*, 2007, **19**, 1239; F. Giannici, A. Longo, A. Balerna and A. Martorana, *Chem. Mater.*, 2009, **21**, 597; M. Oishi, K. Yashiro, K. Sato, J. Mizusaki, N. Kitamura, K. Amezawa, T. Kawada and Y. Uchimoto, *Solid State Ionics*, 2008, **179**, 529.
165 K. S. Knight and N. Bonanos, *J. Mater. Chem.*, 1994, **4**, 899.
166 L. Malavasi, C. Ritter and G. Chiodelli, *Chem. Mater.*, 2008, **20**, 2343.
167 K. S. Knight, *Solid State Ionics*, 2000, **127**, 43–48.
168 T. Pagnier, I. Charrier-Cougoulic, C. Ritter and G. Lucazeau, *Eur. Phys. J.: Appl. Phys.*, 2000, **9**, 1.
169 J. Ranløv, B. Lebech and K. Nielsen, *J. Mater. Chem.*, 1995, **5**, 743.
170 W. Münch, G. Seifert, K. D. Kreuer and J. Maier, *Solid State Ionics*, 1996, **86–88**, 647.
171 F. Shimojo, K. Hoshino and H. Okazaki, *J. Phys. Soc. Jpn.*, 1997, **66**, 8.
172 F. Shimojo and K. Hoshino, *Solid State Ionics*, 2001, **145**, 421.
173 M. Pionke, T. Mono, W. Schweika, T. Springer and T. Schober, *Solid State Ionics*, 1997, **97**, 497.
174 T. Matzke, U. Stimming, C. Karmonik, M. Soetramo, R. Hempelmann and F. Guthoff, *Solid State Ionics*, 1996, **86–88**, 621; R. Hempelmann, M. Soetramo, O. Hartmann and R. Wappling, *Solid State Ionics*, 1998, **107**, 269.
175 G. C. Mather and M. S. Islam, *Chem. Mater.*, 2005, **17**, 1736; M. S. Islam, J. R. Tolchard, P. R. Slater and T. Dinges, *Dalton Trans.*, 2004, 3061; M. Cherry, M. S. Islam, J. D. Gale and C. R. A. Catlow, *Solid State Ionics*, 1995, **77**, 207.
176 W. Münch, K. D. Kreuer, S. Adams, G. Seifert and J. Maier, *Phase Transitions*, 1999, **68**, 567.
177 M. S. Islam, R. A. Davies and J. D. Gale, *Chem. Mater.*, 2001, **13**, 2049.
178 M. Karlsson, D. Engberg, M. E. Bjorketun, A. Matic, G. Wahnstrom, P. G. Sundell, P. Berastegui, I. Ahmed, P. Falus, B. Farago, L. Borjesson and S. Eriksson, *Chem. Mater.*, 2010, **22**, 740.
179 J. Wu, L. P. Li, W. T. P. Espinosa and S. M. Haile, *J. Mater. Res.*, 2004, **19**, 2366; J. Wu, R. A. Davies, M. S. Islam and S. M. Haile, *Chem. Mater.*, 2005, **17**, 846.
180 K. Katahira, Y. Kohchi, T. Shimura and H. Iwahara, *Solid State Ionics*, 2000, **138**, 91.
181 P. Babilo, T. Uda and S. M. Haile, *J. Mater. Res.*, 2007, **22**, 1322; K. H. Ryu and S. M. Haile, *Solid State Ionics*, 1999, **125**, 355; A. R. Akbarzadeh, I. Kornev, C. Malibert, L. Bellaiche and J. M. Kiat, *Phys. Rev. B: Condens. Matter Mater. Phys.*, 2005, **72**, 205104.
182 M. E. Björketun, P. G. Sundell and G. Wahnström, *Phys. Rev. B: Condens. Matter Mater. Phys.*, 2007, **76**, 054307; A. Bilić and J. D. Gale, *Phys. Rev. B: Condens. Matter Mater. Phys.*, 2009, **79**, 174107.
183 P. Babilo and S. M. Haile, *J. Am. Ceram. Soc.*, 2005, **88**, 2362.
184 S. Tao and J. T. S. Irvine, *J. Solid State Chem.*, 2007, **180**, 3493.
185 C. Zuo, S. Zha, M. Liu, M. Datano and M. Uchiyama, *Adv. Mater.*, 2006, **18**, 3318; E. Fabbri, D. Pergolesi, S. Licoccia and E. Traversa, *Solid State Ionics*, 2010, **181**, 1043.
186 S. M. Haile, G. Staneff and K. H. Ryu, *J. Mater. Sci.*, 2001, **36**, 1149; Z. Khani, M. Tallades-Jacquin, G. Taillades, D. J. Jones, M. Marrony and J. Roziere, *Chem. Mater.*, 2010, **22**, 1119.
187 S. Wienströer and H.-D. Wiemhöfer, *Solid State Ionics*, 1997, **101–103**, 1113; A. Bilic and J. D. Gale, *Phys. Rev. B: Condens. Matter Mater. Phys.*, 2009, **79**, 174107; I. Ahmed, M. Karlsson,

S. G. Eriksson, E. Ahlberg, C. S. Knee, K. Larsson, A. K. Azad, A. Matic and L. Borjesson, *J. Am. Ceram. Soc.*, 2008, **91**, 3039; M. E. Bjorketun, P. G. Sundell and G. Wahnstrom, *Faraday Discuss.*, 2007, **134**, 247; A. K. Azad, C. Savaniu, S. W. Tao, S. Duval, P. Holtappels, R. M. Ibberson and J. T. S. Irvine, *J. Mater. Chem.*, 2008, **18**, 3414.
188 X. Xu, S. Tao and J. T. S. Irvine, *J. Solid State Chem.*, 2010, **183**, 93.
189 H. G. Bohn, T. Schober, T. Mono and W. Schilling, *Solid State Ionics*, 1999, **117**, 219.
190 B. Groß, St. Marion, R. Hempelmann, D. Grambole and F. Herrmann, *Solid State Ionics*, 1998, **109**, 13; L. Bi, S. Zhang, S. Fang, L. Zhang, H. Gao, G. Meng and W. Liu, *J. Am. Ceram. Soc.*, 2008, **91**, 3806; W. Wang and A. V. Virkar, *J. Electrochem. Soc.*, 2004, **151**, A1565.
191 I. Animitsa, A. Neiman, A. Sharafutdinov and S. Nochrin, *Solid State Ionics*, 2000, **136–137**, 265.
192 I. Animitsa, A. Nieman, S. Titova, N. Kochetova, E. Isaeva, A. Sharafutdinov, N. Timofeeva and Ph. Colomban, *Solid State Ionics*, 2003, **156**, 95.
193 J. B. Goodenough, J. E. Ruiz-Diaz and Y. S. Zhen, *Solid State Ionics*, 1990, **44**, 21.
194 G. B. Zhang and D. M. Smyth, *Solid State Ionics*, 1995, **82**, 153.
195 S. Noirault, S. Celerier, O. Joubert, M. T. Caldes and Y. Piffard, *Solid State Ionics*, 2007, **178**, 1353; J. F. Shin, L. Hussey, A. Orera and P. R. Slater, *Chem. Commun.*, 2010, 4613.
196 C. E. Mohn, N. L. Allen, C. L. Freeman, P. Ravindran and S. Stølen, *Phys. Chem. Chem. Phys.*, 2004, **6**, 3052; C. E. Mohn, N. L. Allen, C. L. Freeman, P. Ravindran and S. Stølen, *J. Solid State Chem.*, 2005, **178**, 346.
197 C. A. J. Fisher and M. S. Islam, *Solid State Ionics*, 1999, **118**, 355.
198 T. Schober, J. Friedrich and F. Krug, *Solid State Ionics*, 1997, **99**, 9.
199 S. A. Speakman, J. W. Richardson, B. J. Mitchell and S. T. Misture, *Solid State Ionics*, 2002, **149**, 247.
200 C. A. J. Fisher, B. Derby and R. J. Brook, in *Oxygen Ion Conductors and their Technological Applications*, ed. B. C. H. Steele, British Ceramic Proceedings, Institute of Materials, Cambridge, 1996, vol. 56, pp. 25–33.
201 K. Kakinuma, A. Tomita, H. Yamamura and T. Atake, *J. Mater. Sci.*, 2006, **41**, 6435.
202 E. Quarez, S. Noirault, M. T. Caldes and O. Joubert, *J. Power Sources*, 2010, **195**, 1136.
203 T. Norby and N. Christiansen, *Solid State Ionics*, 1995, **77**, 240.
204 K. Amezawa, S. Kjelstrup, T. Norby and Y. Ito, *J. Electrochem. Soc.*, 1998, **145**, 3313.
205 K. Amezawa, Y. Tomii and N. Yamamoto, *Solid State Ionics*, 2004, **175**, 569.
206 K. Amezawa, Y. Kitajima, Y. Tomii, N. Yamamoto, M. Widerøe and T. Norby, *Solid State Ionics*, 2005, **176**, 2867.
207 D. A. Boysen, T. Uda, C. R. I. Chisholm and S. M. Haile, *Science*, 2004, **303**, 68; S. M. Haile, D. A. Boysen, C. R. I. Chisholm and R. B. Merle, *Nature*, 2001, **410**, 910.
208 R. Haugsrud and T. Norby, *Nat. Mater.*, 2006, **5**, 193.
209 R. Haugsrud and T. Norby, *Solid State Ionics*, 2006, **177**, 1129.
210 L. Malavasi, C. Ritter and G. Chiodelli, *J. Alloys Compd.*, 2009, **475**, L42.
211 R. Haugsrud and T. Norby, *J. Am. Ceram. Soc.*, 2007, **90**, 1116.
212 R. Haugsrud, B. Ballesteros, M. Lira-Cantú and T. Norby, *J. Electrochem. Soc.*, 2006, **153**, J87; H. Fjeld, D. M. Kepaptsoglou, R. Haugsrud and T. Norby, *Solid State Ionics*, 2010, **181**, 104.
213 A. Kuwabara, R. Haugsrud, S. Stølen and T. Norby, *Phys. Chem. Chem. Phys.*, 2009, **11**, 5550.
214 M. Arai, Y. X. Wang, S. Kohiki, M. Matsuo, H. Shimooka, T. Shishido and M. Oku, *Jpn. J. Appl. Phys.*, 2005, **44**, 6596.
215 M.-L. Fontaine, Y. Larring, R. Haugsrud, T. Norby, K. Wiik and R. Bredesen, *J. Power Sources*, 2009, **188**, 106.
216 T. Norby and Y. Larring, *Curr. Opin. Solid State Mater. Sci.*, 1997, **2**, 593.
217 N. Kitamura, T. Usuki and Y. Idemoto, *Electrochemistry*, 2009, **77**, 158.